JCB Journal of Cell Biology

ARTICLE

Regulated resurfacing of a somatostatin receptor storage compartment fine-tunes pituitary secretion

Walaa Alshafie, Vincent Francis, Klaudia Bednarz, Yingzhou Edward Pan, Thomas Stroh, and Peter S. McPherson

The surfacing of the glucose transporter GLUT4 driven by insulin receptor activation provides the prototypic example of a homeostasis response dependent on mobilization of an intracellular storage compartment. Here, we generalize this concept to a G protein–coupled receptor, somatostatin receptor subtype 2 (SSTR2), in pituitary cells. Following internalization in corticotropes, SSTR2 moves to a juxtanuclear syntaxin-6–positive compartment, where it remains until the corticotropes are stimulated with corticotropin releasing factor (CRF), whereupon SSTR2 exits the compartment on syntaxin-6–positive vesicular/tubular carriers that depend on Rab10 for their fusion with the plasma membrane. As SSTR2 activation antagonizes CRF-mediated hormone release, this storage/resurfacing mechanism may allow for a physiological homeostatic feedback system. In fact, we find that SSTR2 moves from an intracellular compartment to the cell surface in pituitary gland somatotropes, concomitant with increasing levels of serum growth hormone (GH) during natural GH cycles. Our data thus provide a mechanism by which signaling-mediated plasma membrane resurfacing of SSTR2 can fine-tune pituitary hormone release.

Introduction

The hypothalamic–pituitary axis is a major neuroendocrine system regulating a myriad of physiological processes, including growth, digestion, stress, energy expenditure, mood and emotions, and sexuality. Neurons in the hypothalamus release protein factors that bind to distinct stimulatory receptors on each of the five major cell types of the anterior pituitary, stimulating hormone release from the pituitary cells. The pituitary cell types include somatotropes that release growth hormone (GH) and corticotropes that release adrenocorticotropic hormone (ACTH; Cuevas-Ramos and Fleseriu, 2014; Eigler and Ben-Shlomo, 2014). Each pituitary cell type also expresses somatostatin receptor subtype 2 (SSTR2), the major receptor mediating the physiological regulatory actions of the neuropeptide somatostatin (SOM; Martel et al., 2012). Activation of SSTR2 by SOM, released from the paraventricular nuclei of the hypothalamus (Eigler and Ben-Shlomo, 2014), antagonizes the stimulatory actions of the pituitary receptors that respond to the hypothalamic releasing factors. For example, GH releasing hormone (GHRH) binds to the GHRH receptor on the surface of somatotropes, stimulating the release of GH. These actions are inhibited by activation of SSTR2 on the somatotropes. The importance of SSTR2 activation on the control of GH release is highlighted by the fact that SSTR2 agonists are used clinically for treatment of acromegaly, which is caused by excessive release of GH from pituitary adenomas (Cheung and Boyages, 1995; Lopez et al., 1996; Peverelli et al., 2017).

GH release from somatotropes occurs with an ultradian rhythm that is thought to be established through the pulsatile release of GHRH from hypothalamic neurons, coupled to the antagonizing action of SOM (Frohman et al., 1990; Plotsky and Vale, 1985; Richardson and Twente, 1993; Tannenbaum et al., 1990). However, the mechanisms by which SOM contributes to the normal rhythms of hormone release remain unclear. Specifically, since SSTR2 is found on all pituitary cell types, which release hormones with unique patterns, it is difficult to envision how SOM release could be coordinated to fine-tune each of these hormone release cycles.

SSTR2 inhibits the ability of the stimulating factor receptors to induce hormone secretion by suppressing their downstream signaling pathways (Eigler and Ben-Shlomo, 2014). It is likely that the releasing factor receptors feedback and regulate SSTR2 functionality. Potential mechanisms for this regulation include direct interaction of the stimulatory receptors with SSTR2, modulation of SSTR2 sensitivity to ligand binding, alterations in SSTR2 downstream signaling pathways, or changes in the cellular localization of SSTR2 through altering its membrane trafficking/cellular localization.

Department of Neurology and Neurosurgery, Montreal Neurological Institute, McGill University, Montreal, Quebec, Canada.

Correspondence to Peter S. McPherson: peter.mcpherson@mcgill.ca; Thomas Stroh: thomas.stroh@mcgill.ca.

https://doi.org/10.1083/jcb.201904054

SSTR2 and the stimulating factor receptors are all members of the G protein–coupled receptor (GPCR) superfamily, the largest family of plasma membrane receptors and major therapeutic targets for many pathophysiological conditions. As for other GPCRs, SSTR2 activation in response to its ligand induces receptor phosphorylation (Lehmann et al., 2014) that allows for interaction with β-arrestins (Tulipano et al., 2004), driving its recruitment to clathrin-coated pits for endocytosis (Brasselet et al., 2002; Mundell and Benovic, 2000; Tulipano et al., 2004). In general, endocytosis of GPCRs is a mechanism to regulate G protein signaling. Following delivery to endosomes, the internalized receptor can recycle back to the plasma membrane in an active form for further rounds of signaling, or it can remain in the body of the endosomes, which mature into lysosomes for receptor degradation.

Following endocytosis, SSTR2 traffics to a juxtanuclear compartment that is positive for syntaxin-6 (Csaba et al., 2007). Here, we verify that SSTR2 recycles from this compartment but with remarkably slow kinetics. We have used a combination of standard and superresolution microscopy, live-cell imaging, treatment with the fungal toxin Brefeldin A, and subcellular fractionation to demonstrate that this compartment is distinct from the TGN and shares multiple characteristics with GLUT4 vesicles. In response to insulin receptor activation in muscle and fat cells, GLUT4 vesicles are mobilized in a Rab10-dependent manner to the cell surface where they fuse, allowing for GLUT4-dependent uptake of glucose (Belman et al., 2014; Sano et al., 2007; Vazirani et al., 2016). We now find that in corticotropes, stimulation of the corticotropin releasing factor (CRF) receptor causes rapid, Rab10-dependent resurfacing of previously endocytosed SSTR2, providing a feedback mechanism to inhibit CRF receptor signaling. Moreover, we extend this observation to regulation of natural cycles of pulsatile GH release in mice. This membrane trafficking mechanism provides a unique and unexpected means for regulating GPCR responsiveness in the pituitary gland and fine-tuning rhythms of hormone release.

Results

SSTR2 traffics from the cell surface to a syntaxin-6–enriched compartment via an endosomal pathway

Given the key role of SSTR2 activation in inhibiting hormone secretion in pituitary cells, we sought to better understand the receptor's trafficking itinerary, as this could allow for the discovery of new regulatory mechanisms in pituitary function. We used the corticotrope cell line AtT20 that expresses CRF receptor and SSTR2 endogenously. To induce SSTR2 trafficking, we stimulated the cells with [D-Trp^8]-SOM, a stable form of SOM. We compared the localization of SSTR2 to that of fluorescent transferrin (Trf), which binds the Trf receptor and marks early/recycling endosomes after receptor internalization (Trischler et al., 1999), and with syntaxin-6, as SSTR2 is known to traffic to a syntaxin-6–positive juxtanuclear compartment (Csaba et al., 2007). Cells were placed on ice to prevent all membrane trafficking and incubated with Trf and [D-Trp^8]-SOM before shifting to 37°C. At 0 min (cells remained on ice), Trf and SSTR2 fluorescent signals were confined to the cell surface, while syntaxin-6 revealed a juxtanuclear concentration (Fig. 1, A–C). At 5 min, SSTR2 was internalized and partially colocalized with Trf in syntaxin-6–negative endosomes and partially with syntaxin-6 in a compartment devoid of Trf labeling (Fig. 1, A–C). At 40 min, SSTR2 was prominent in a syntaxin-6–labeled juxtanuclear compartment, while some receptor remained in Trf-positive endosomes (Fig. 1, A–C). The appearance of SSTR2 in the syntaxin-6–positive compartment was dependent on endocytosis, as it was blocked by treatment of cells with dynasore or hypertonic sucrose (Fig. 1, D and E).

SSTR2 recycles from the syntaxin-6 compartment with slow kinetics

The removal of a GPCR from the plasma membrane desensitizes cells to further ligand stimulation and the length of this refractory period is important in sculpting cellular responses. Certain GPCRs have developed mechanisms based on their trafficking itinerary to control their recycling rate. For example, glucose-dependent insulinotropic polypeptide receptor can switch from fast, endosome-based recycling to a slower recycling pathway after shifting to the TGN (Abdullah et al., 2016). We sought to test if SSTR2 recycles from the syntaxin-6 compartment and, if so, at what rate. We thus stimulated AtT20 cells with [D-Trp^8]-SOM for 40 min and then removed the ligand allowing for recycling. While SSTR2 did recycle from the syntaxin-6 compartment, it did so with extremely slow kinetics (Fig. 2, A and B). Only 25% of internalized SSTR2 recycled back to the cell surface 1 h after agonist washout, with the number rising to 39% after 4 h and 82% after 24 h (Fig. 2 B). Brefeldin A treatment, which disrupts the TGN (Reaves and Banting, 1992; Tallent et al., 1996; Wood et al., 1991), did not significantly change the slow recycling dynamics of SSTR2 (Figs. 2 B and S1 A), suggesting that the receptor is not stored at the TGN. Additionally, cycloheximide treatment does not prevent the recycling of SSTR2 (Fig. S1 B), indicating that the return of the receptor to the surface does not depend upon newly synthesized receptor, consistent with the concomitant loss of SSTR2 from the syntaxin-6 compartment (Figs. 2 A and S1 B). Given these slow recycling dynamics, we sought to investigate the nature of the juxtanuclear syntaxin-6–positive SSTR2 compartment.

The syntaxin-6–positive SSTR2 compartment is distinct from the TGN

Syntaxin-6 has been widely used as a marker of the TGN, leading to the conclusion that SSTR2 is trafficked to the TGN following internalization (Csaba et al., 2007). However, the fact that Brefeldin A treatment does not alter the slow recycling dynamics of SSTR2 (Figs. 2 and S1) is not consistent with this conclusion. To reexamine this issue, we first used standard confocal microscopy to compare the localization of internalized SSTR2 to that of syntaxin-6 and the reported TGN marker, a protein interacting specifically with Tc10 (PIST; Yao et al., 2001). After 40 min of internalization, SSTR2 demonstrates extensive colocalization with syntaxin-6 but limited colocalization with PIST (Figs. 3 A and S2 E). Consistently, there is little overlap between PIST and syntaxin-6, whereas PIST shows extensive colocalization with

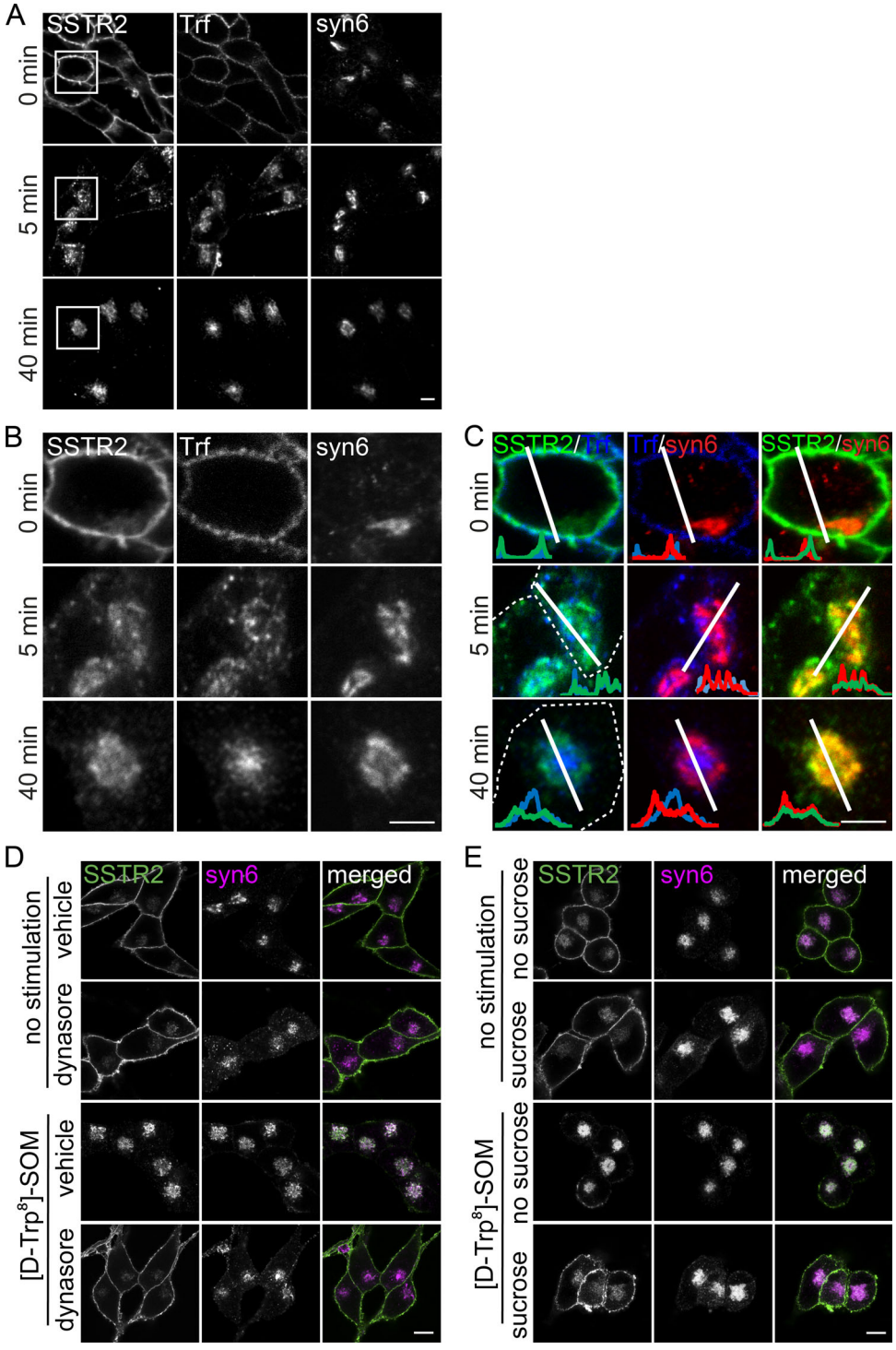

Figure 1. **Following internalization SSTR2 traffics to a syntaxin-6–positive compartment through an endosomal pathway. (A–C)** AtT20 cells were serum starved for 2 h and then transferred to ice. The cells were incubated on ice for 1 h in the presence of 5 µg/ml Alexa Fluor 647–labeled Trf and 100 nM [D-Trp^8]-SOM. Cells were than fixed (0 min) or transferred to 37°C for either 5 or 40 min as indicated before being fixed and processed for immunofluorescence with antibodies recognizing SSTR2 and syntaxin-6. Images were acquired using a LSM 710 confocal microscope. The images in B and C correspond to the boxed areas in A. For C, the intensity distributions for the lines passing through the images are indicated. Scale bars represent 10 µm in A and 5 µm in B and C. **(D)** AtT20 cells were washed extensively with Earle's buffer and then incubated with 80 µM dynasore or vehicle control for 20 min before and during a 40-min incubation without (no stimulation) or with 100 nM [D-Trp8]-SOM at 37°C. Cells were than fixed and processed for immunofluorescence with antibodies recognizing SSTR2 and syntaxin-6. **(E)** Sucrose (0.45 M) was added to cells in Earle's buffer and incubated for 15 min before and during a 40-min stimulation without (no stimulation) or with 100 nM of [D-Trp^8]-SOM at 37°C. The stimulation was ended by washing in ice-cold Earle's buffer and the cells were processed for immunofluorescence with antibodies recognizing SSTR2 and syntaxin-6. Images were acquired using the superresolution mode of the LSM 880 confocal microscope. Scale bars represent 5 µm.

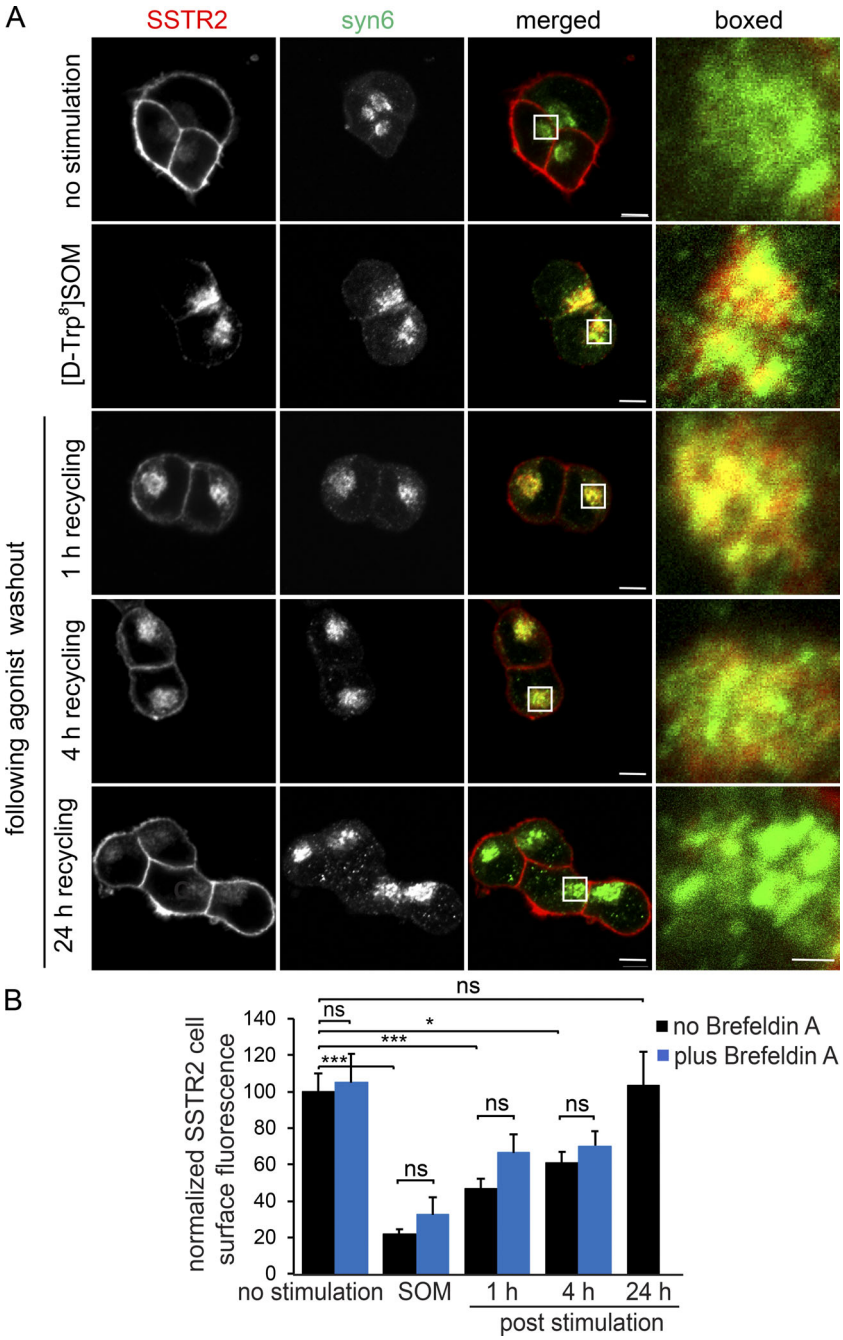

Figure 2. **SSTR2 displays slow recycling kinetics. (A)** AtT20 cells were incubated for 40 min without (no stimulation) or with 100 nM [D-Trp^8]-SOM and then fixed and processed for immunofluorescence with antibodies recognizing SSTR2 or syntaxin-6 (top two rows of panels). In parallel, cells treated with 100 nM [D-Trp^8]-SOM for 40 min were subsequently transferred to 4°C, surface-bound agonist was stripped by a brief acid wash, and the cells were returned to 37°C for 1, 4, or 24 h before being processed for immunofluorescence with antibodies recognizing SSTR2 or syntaxin-6 (bottom three rows of panels). The boxes in the merged images are shown at higher magnification on the far right. Scale bars represent 5 µm and 1 µm for the low and high magnifications, respectively. **(B)** Quantification of SSTR2 cell surface immunofluorescence intensity from three successive experiments as shown in A and from three parallel experiments in the presence of Brefeldin A as shown in Fig. S1 with 10–15 cells quantified per condition per experiment. Data were analyzed by two-way ANOVA and Bonferroni comparison test (and procedures implemented in GraphPad statistical package). Data are presented as least-square means ± SEMs with treatment effects significant at 0.05. *, P ≤ 0.05; ***, P ≤ 0.001.

another TGN-enriched protein, TGN38 (Luzio et al., 1990; Figs. 3 B and S2 E). Additionally, we took advantage of the microtubule-depolymerizing drug nocodazole, which induces polarized Golgi ministacks, simplifying visualization of the Golgi complex (Tie et al., 2016). In the presence of nocodazole, SSTR2 continues to show extensive colocalization with syntaxin-6, and the TGN markers PIST and TGN38 remain colocalized (Fig. S2, A, B, and F). In contrast, PIST shows markedly less colocalization with the cis-Golgi protein Giantin or syntaxin-6 (Fig. S2, C, D, and F).

To further examine the relationship between the syntaxin-6–positive compartment and the TGN, we used stimulated emission depletion (STED) microscopy, which overcomes the diffraction limit of standard light microscopy. For example, SSTR2 internalized after 3 min of incubation with SOM appears as a series of clusters in standard confocal microscopy but resolves into individual vesicular structures in STED microscopy (Fig. 3 C). Following 40 min of internalization, STED reveals that the juxtanuclear cluster of SSTR2 is composed of distinct tubular/vesicular structures, as is the syntaxin-6 compartment (Fig. 3, D and E). Moreover, direct colocalization studies using STED reveals overlap of internalized SSTR2 with syntaxin-6 but segregation of SSTR2 from PIST (Fig. 3 F). Moreover, syntaxin-6 shows little colocalization with either TGN38 or PIST (Fig. 3 G).

Brefeldin A treatment causes the Golgi apparatus to collapse into the endoplasmic reticulum and induces tubulation and dispersion of the TGN (Lippincott-Schwartz et al., 1991; Reaves

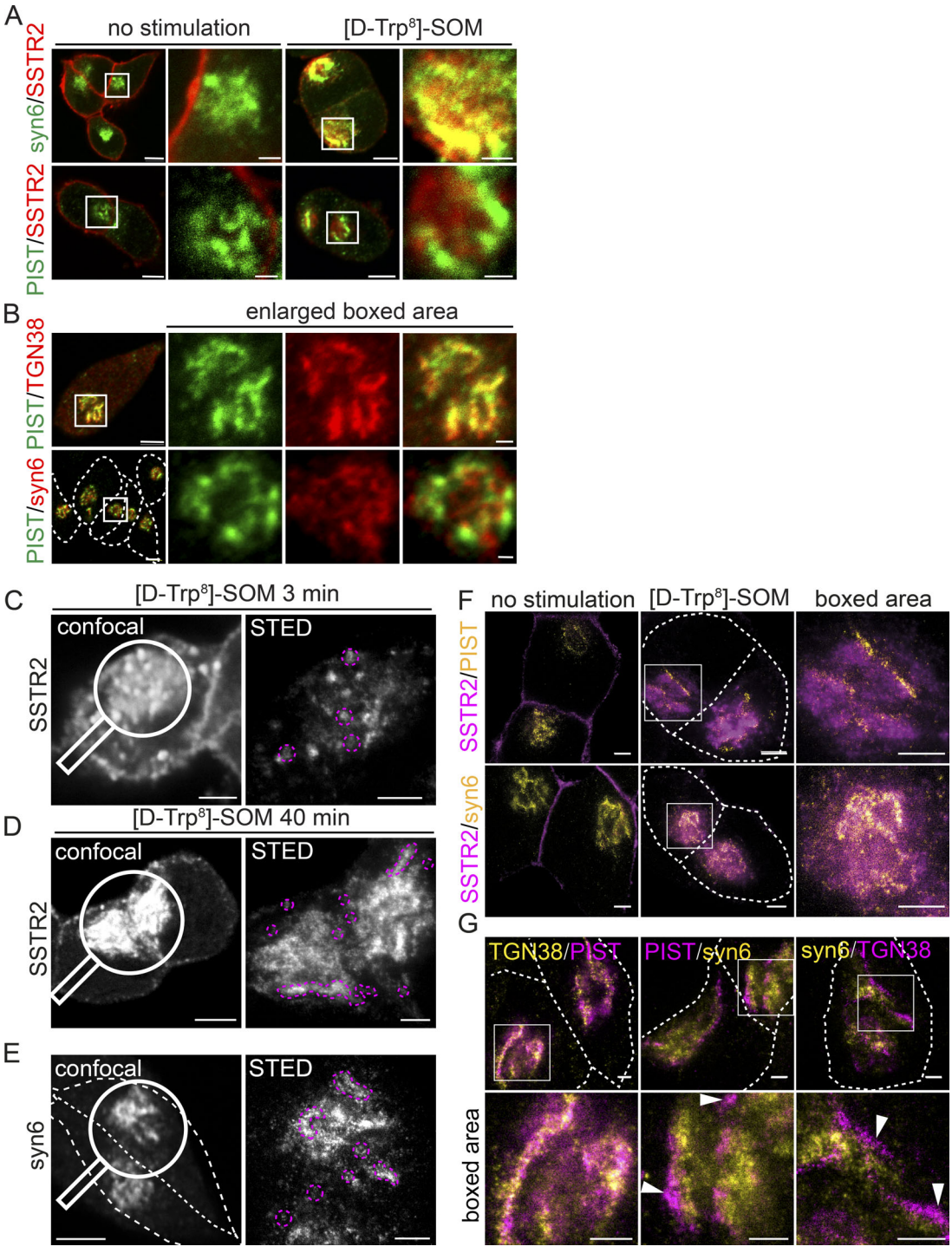

Figure 3. **Confocal and STED microscopy reveals that internalized SSTR2 localizes to a cellular compartment distinct from the TGN. (A)** AtT20 cells were incubated for 40 min without (no stimulation) or with 100 nM [D-Trp^8]-SOM and then fixed and processed for immunofluorescence with antibodies recognizing the indicated proteins. The boxed areas are shown at higher magnification to the right for each treatment condition. Scale bars represent 5 µm and 1 µm for the lower and higher magnification images, respectively. **(B)** AtT20 cells were fixed and processed for immunofluorescence with antibodies recognizing the indicated proteins. The boxed areas are shown at higher magnification to the right for each set of images. Scale bars represent 5 µm and 1 µm for the lower and higher magnification images, respectively. Dotted lines indicate the plasma membrane. **(C)** AtT20 cells were incubated for 3 min with 100 nM [D-Trp^8]-SOM and then fixed and processed for immunofluorescence with antibodies recognizing SST2R. Images were collected using standard confocal microscopy, and the area under the magnifying glass was acquired by STED microscopy. Scale bars represent 5 µm and 1 µm for the confocal and STED images, respectively. Dashed areas in the STED image indicate individual SSTR2-labeled vesicles. **(D and E)** AtT20 cells were incubated for 40 min with 100 nM [D-Trp^8]-SOM and then fixed and processed for immunofluorescence with antibodies recognizing SSTR2 (D) or syntaxin-6 (E). Images were collected using standard confocal microscopy and the area under the magnifying glass was acquired by STED microscopy. Scale bars represent 5 µm and 1 µm for the confocal and STED images, respectively. Dashed lines in the confocal image indicate the cell boundary and dashed lines in the STED image indicate tubulovesicular

structures. **(F)** AtT20 cells were incubated for 40 min without (no stimulation) or with 100 nM [D-Trp^8]-SOM and then fixed and processed for immunofluorescence with antibodies recognizing the indicated proteins. The boxed areas are shown at higher magnification to the right for the [D-Trp^8]-SOM treatment condition. Scale bars represent 5 µm and 1 µm for the lower and higher magnification images, respectively. Images were acquired using an Abberior STED microscope as a single optical section through the cells and cropped using ImageJ. Dashed lines indicate cell boundaries. **(G)** AtT20 cells were fixed and processed for immunofluorescence with antibodies recognizing the indicated proteins. The boxed areas are shown at higher magnification in the bottom row for each image. Scale bars represent 5 µm and 1 µm for the lower and higher magnification images, respectively. Images were acquired using an Abberior STED microscope as a single optical section through the cells and cropped using ImageJ. Dashed lines indicate cell boundaries. The arrowheads indicate the spatial segregation of immunoreactive signals of the indicated proteins.

and Banting, 1992; Wood et al., 1991). Treatment of AtT20 cells with 10 µM Brefeldin A for 40 min led to dispersion of both PIST and TGN38 into the cytoplasm, whereas syntaxin-6 staining retained its clustered, juxtanuclear localization (Fig. 4 A). The lack of influence of Brefeldin A on syntaxin-6 distribution, in the face of complete redistribution of TGN markers, was also observed in primary neurons (Fig. 4 B), C2C12 myoblasts (Fig. 4 C), and HEK-293, HeLa, and MCF10A cells (Fig. 4, G–I). Importantly, the juxtanuclear pool of SSTR2 resulting from SOM treatment did not disperse following subsequent treatment with Brefeldin A (Fig. 4, D and E). Moreover, internalized SSTR2 had minimal colocalization with the Brefeldin A dispersed PIST immunolabeling but remained well colocalized with syntaxin-6 under Brefeldin A treatment (Fig. 4, D–F). Taken together, these studies indicate that a large proportion of the overlapping SSTR2 and syntaxin-6 signals are spatially distinct from the TGN, suggesting a unique syntaxin-6–positive SSTR2 compartment.

Biochemical segregation of the TGN from the syntaxin-6/SSTR2 compartment

As an independent means to verify segregation of the syntaxin-6/SSTR2 compartment from the TGN, we used subcellular fractionation. We used anti-HA magnetic beads to immunoisolate syntaxin-6–positive structures from HEK-293 cells cotransfected with HA-tagged syntaxin-6 and T7-SSTR2. Both endogenous syntaxin-6 and tagged SSTR2 were enriched on the immunopreciptated structures as compared with the input cell lysate, whereas PIST and TGN46 were not enriched on those structures (Fig. 5 A). We additionally fractionated lysates of AtT20 cells on sucrose density gradients. Whereas the syntaxin-6 signal is concentrated in fractions 12–20, PIST and TGN38 are confined to fractions 4–10, and the cis-Golgi protein GM130 is restricted to fractions 8–10 (Fig. 5 B). Taken together, the immunolocalization and subcellular fractionation studies reveal that internalized SSTR2 traffics to a syntaxin-6–positive compartment that is distinct from the TGN.

Characterization of the syntaxin-6–positive SSTR2 compartment

We next sought to characterize the syntaxin-6/SSTR2 compartment using stochastic optical reconstruction microscopy (STORM) to determine compartment size and live cell imaging to examine compartment dynamics. STORM is a single molecule localization nanoscopy technique that takes advantage of photoswitchable fluorescent probes and their probabilistic excitation and transition to a dark state to spatially isolate individual molecules. Determining the precise localization of individual fluorophores in thousands of frames allows for a superresolved image with near molecular resolution. We used STORM to localize SSTR2 in relation to syntaxin-6 to provide insight into the size of the compartment. With STORM, the pattern of SSTR2 in cells at the basal level versus cells stimulated with SOM was similar to that obtained with other imaging modalities (Fig. 6 A). We hypothesized that internalized SSTR2 and syntaxin-6 are on the same vesicles, however, because the labeling and/or the probes are not uniformly distributed across the vesicle shell, it is difficult to identify vesicular structures unequivocally in the STORM images. To address this, we used nearest-neighbor analysis to estimate the distances between SSTR2 and syntaxin-6 at both the juxtanuclear compartment or throughout the rest of the cell (cytoplasm and plasma membrane) as described (Fig. 6 G). In the juxtanuclear compartment, the vast majority of syntaxin-6 molecules were within 55 nm of their nearest SSTR2 neighbor (Fig. 6 B). Particle counts were highest following stimulation with SOM. No syntaxin-6 molecules were ≥200 nm from SSTR2 molecules, indicating confined structures. This differs from the random distribution observed for the proteins PIST and Giantin (Fig. 6, B and H), which are known to reside on different compartments. In the rest of the cell (cytoplasm and plasma membrane), the most frequent distances between syntaxin-6 and the nearest SSTR2 localizations were between 55 and 100 nm, with no events observed at distance ≥300 nm (Fig. 6 C). These observations indicate that SSTR2 and syntaxin-6 colocalize on vesicular structures of <100 nm diameter. Importantly, the nearest-neighbor analysis for SSTR2 and PIST shows random distribution similar to that observed for PIST and Giantin (Fig. 6, D–F).

We next characterized the SSTR2/syntaxin-6 compartment using live-cell imaging in HeLa cells. At 48 h following transfection, EGFP-SSTR2 accumulates on the plasma membrane (Fig. 7 A and Video 1), similar to endogenous protein in AtT20 cells. Upon treatment with SOM, the receptor is internalized into a juxtanuclear compartment (Fig. 7 A and Video 2), and following SOM washout, SSTR2 recycles back to the plasma membrane, mostly within 30 min (Fig. 7 A and Video 3). Thus, the trafficking itinerary of SSTR2 in HeLa cells is similar to the endogenous protein in AtT20 cells with the exception that recycling is much faster. This suggests that there are factors in AtT20 cells that constrain recycling that are absent in HeLa cells, which lack endogenous SSTR2. Importantly, as in AtT20 cells, the SSTR2 juxtanuclear compartment in HeLa cells is positive for syntaxin-6 (Fig. 7 B). By tracking the dynamics of SSTR2 and dsRed-syntaxin-6 in live-cell experiments, we observe that SSTR2 leaves the compartment in syntaxin-6–positive carriers that traffic toward the plasma membrane (Fig. 7 B, box a; and

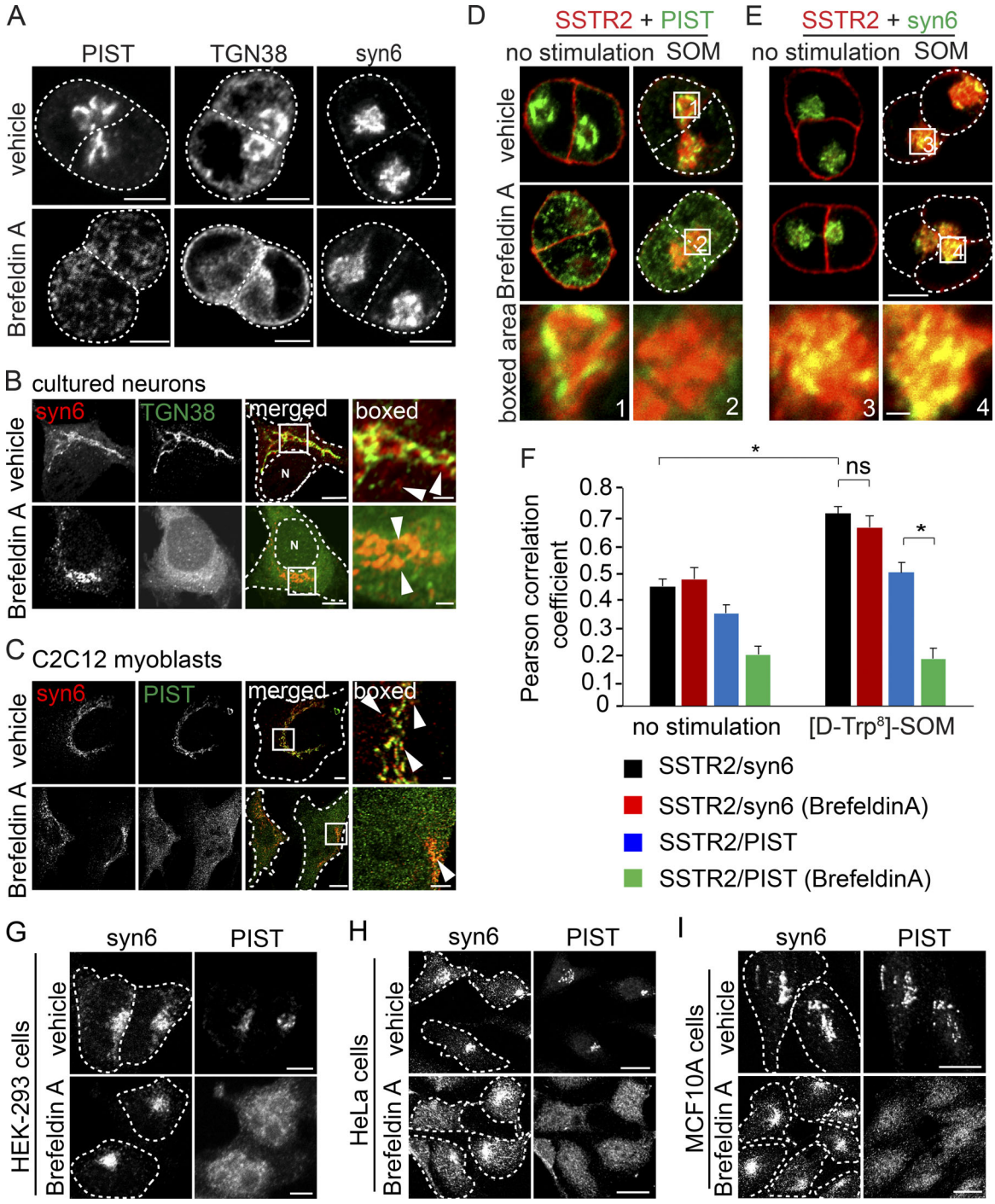

Figure 4. **The SSTR2/syntaxin-6 compartment is resistant to Brefeldin A treatment. (A–C)** AtT20 cells (A), cultures of primary cortical neurons (B), and C2C12 myoblasts (C) were incubated with vehicle control or Brefeldin A for 40 min before fixation and processing for immunofluorescence with antibodies recognizing the indicated antibodies. For B and C, the areas indicated by boxes in the merged images are shown at higher magnification on the right. Arrowheads represent nonoverlapping signals. For all images, scale bars represent 5 µm and 1 µm for the low- and high-magnification images, respectively, and the dashed lines indicate cell boundaries. The outline of the nucleus (N) is also indicated by a dashed line in B. **(D and E)** AtT20 cells were incubated for 15 min with vehicle control or Brefeldin A before the 40-min stimulation of [D-Trp^8]-SOM. The cells were then fixed and processed for immunofluorescence with antibodies recognizing the indicated proteins. The boxed areas are shown at higher magnification in the bottom sets of panels. The dashed lines indicate cell boundaries. Scale bars represent 5 µm and 1 µm for the low- and high-magnification images, respectively. **(F)** Pearson coefficient measurement of SSTR2/syntaxin-6 or SSTR2/PIST colocalization in a juxtanuclear ROI. The quantification is based on 40–60 cells per condition from four successive, independent experiments. Data were analyzed by one1-factor ANOVA and Tukey comparison test (procedures implemented in JMP statistical package; SAS Institute). Data are presented as least-square means ± SEMs with treatment effects significant at *, $P < 0.05$. **(G–I)** HEK-293 cells (G), HeLa cells (H), and MCF10A cells (I) were incubated with vehicle control or Brefeldin A for 40 min before fixation and processing for immunofluorescence using antibodies recognizing the indicated antibodies. Scale bars represent 5 µm. The dashed lines indicate cell boundaries.

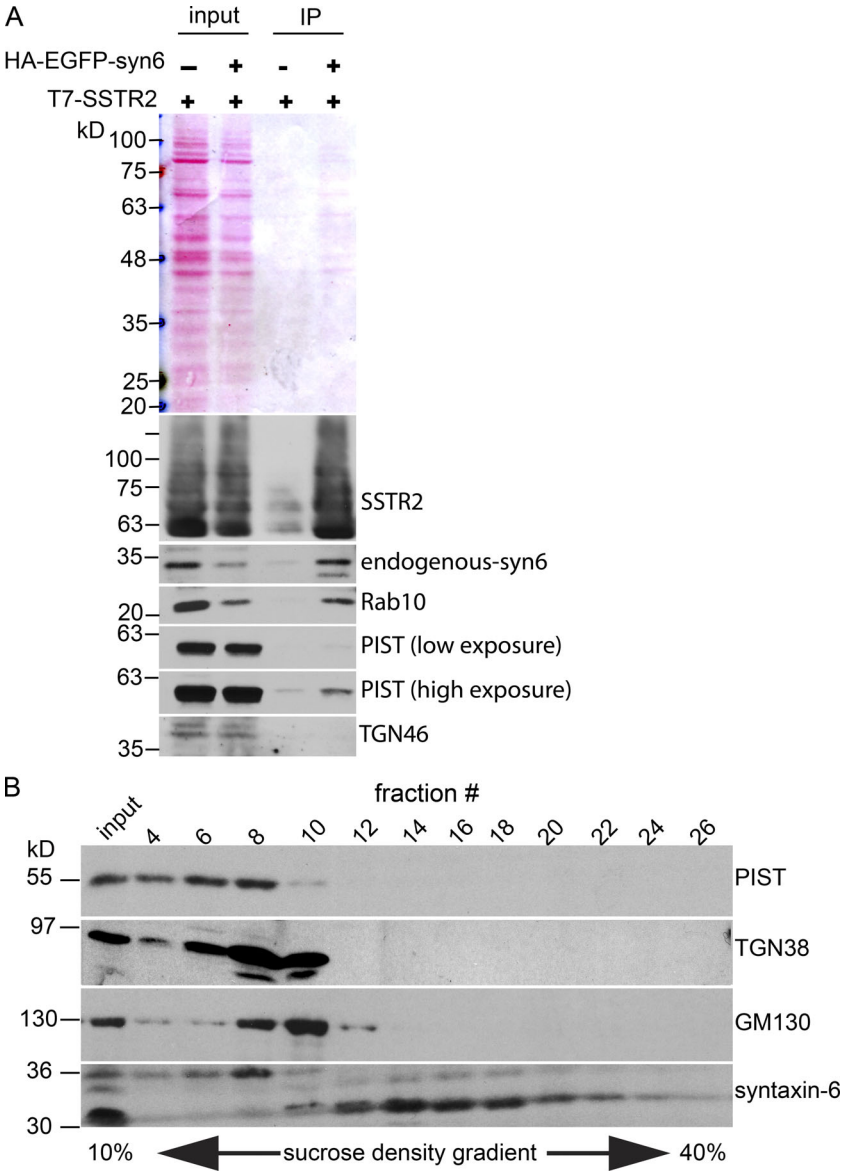

Figure 5. **SSTR2 fractionates with a syntaxin-6 compartment distinct from the TGN. (A)** Immunoisolation of syntaxin-6–positive vesicles. HEK-293 cells were transfected with T7-SSTR2 alone or in combination with HA-EGFP-syntaxin-6. Cell lysates were prepared in detergent free buffer, and HA-EGFP-syntaxin-6 structures were isolated using anti-HA magnetic beads. The proteins were separated by SDS-PAGE and probed by immunoblot using antibodies recognizing the indicated proteins. The migration of molecular weight markers in kilodaltons is indicated. IP, immunoprecipitate. **(B)** Sucrose gradient separation of the syntaxin-6 compartment. 2 ml of AtT20 postnuclear supernatant collected from three 10-cm dishes was fractionated on a 10-ml continuous 10–40% (wt/vol) sucrose density gradient. Fractions (500 µl) were harvested, beginning at the top of the gradient. Equal volumes from every other fraction were separated by SDS-PAGE and processed for immunoblot using antibodies against recognizing PIST, TGN38, GM130, and syntaxin-6. *n* = 4. The migration of molecular weight markers in kilodaltons is indicated.

Video 4). Upon reaching the surface, the carriers can be seen to come in contact with the membrane followed by the movement of SSTR2 into the plasma membrane, while syntaxin-6 remains on the cytoplasmic face of the plasma membrane (Fig. 7 B, box b; and Video 5). SSTR2 can also be seen to recycle on tubular structures that fuse with the plasma membrane (Fig. 7 C and Video 6).

SSTR2 is sequestered in GLUT4-like storage vesicles (GLSVs)

We have thus far observed that in AtT20 corticotropes, internalized SSTR2 resides in a syntaxin-6–positive intracellular storage compartment from where it can recycle to the surface but with slow kinetics. The compartment is composed of vesicles centered ∼55 nm in diameter, and in HeLa cells, the recycling has much faster kinetics than in AtT20 cells, indicating that the storage compartment is specialized. Moreover, the distribution of the compartment and trafficking from the compartment are insensitive to Brefeldin A. These observations are reminiscent of GLUT4 storage vesicles (GSVs) that are specialized for the storage and resurfacing of GLUT4 in specific cell types, notably myocytes and adipocytes (Jaldin-Fincati et al., 2017; Zhou et al., 2017). GSVs are positive for syntaxin-6 (Foley and Klip, 2014; Shewan et al., 2003) and are 50–80 nm in diameter, and their sequestration in a juxtanuclear compartment is insensitive to Brefeldin A (Bao et al., 1995; Chakrabarti et al., 1994; Martin et al., 2000). In response to high blood glucose, increased insulin activates insulin receptor signaling pathways that mobilize GSVs to the surface where they fuse, placing GLUT4 on the surface and allowing for glucose uptake (Belman et al., 2014; Vazirani et al., 2016). Interestingly, in adipocytes, this process is dependent on the small GTPase Rab10 (Sano et al., 2007; Vazirani et al., 2016). We thus hypothesized that GLSVs are involved in the storage and recycling of SSTR2, leading us to test if SSTR2 can be mobilized to the cell surface in response to an appropriate physiological ligand and if such mobilization is Rab10 dependent.

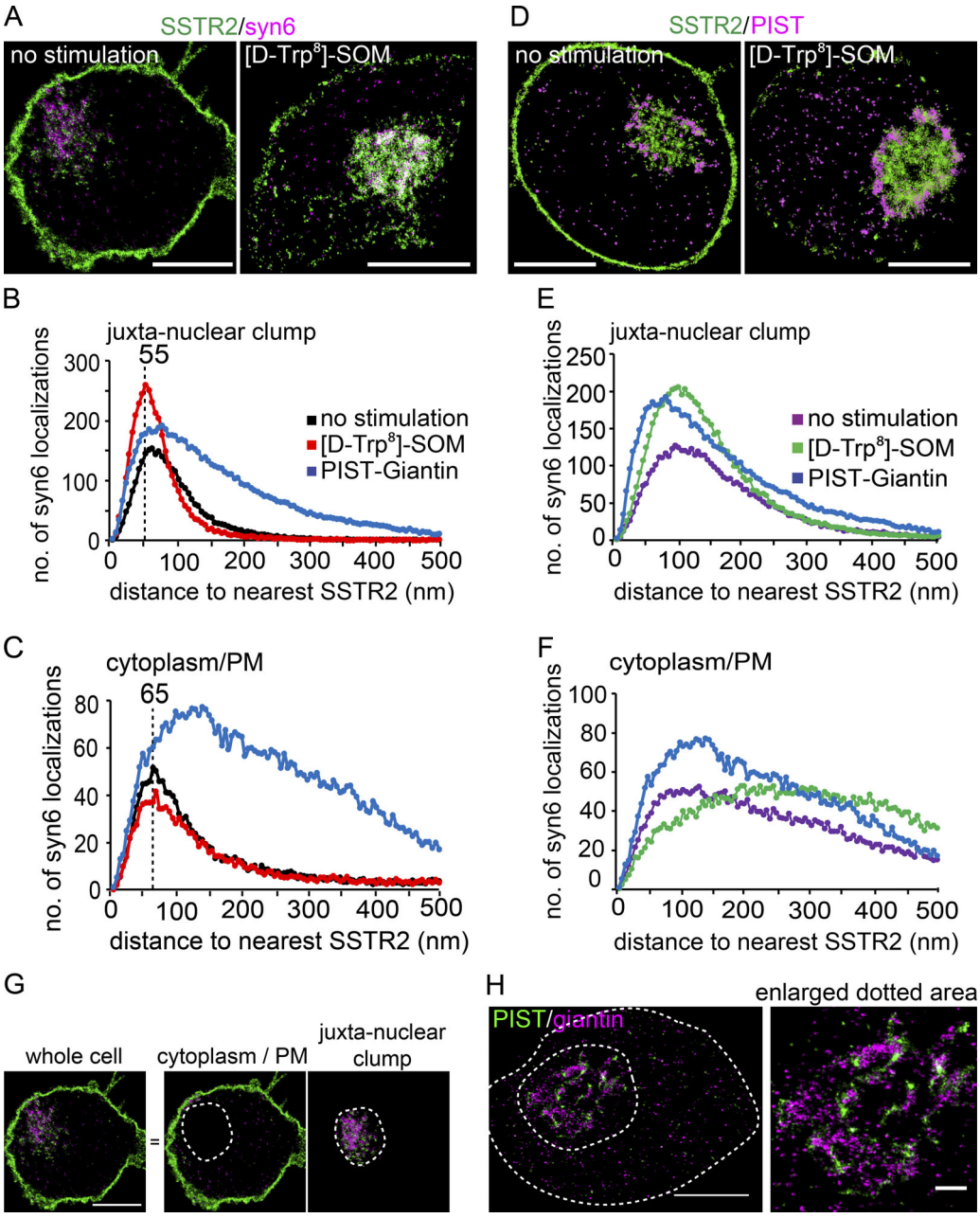

Figure 6. **STORM of SSTR2. (A and D)** AtT20 cells were left at steady state (no stimulation) or incubated with 100 nM [D-Trp^8]-SOM for 60 min. **(A)** Cells were immunostained for SSTR2 and syntaxin-6 and (B) for SSTR2 and PIST. Cross-nearest-neighbor measurements are shown between SSTR2 and syntaxin-6 versus the spatially unrelated proteins PIST and Giantin (B and C) or for SSTR2 and PIST versus PIST and Giantin (E and F). PM, plasma membrane. Note the increase in spatial association between SSTR2 and syntaxin-6 following [D-Trp^8]-SOM stimulation in the juxtanuclear clump in B but the random distribution of SSTR2 and PIST in E. Images were acquired using a Vutara SR-350 Biplane point-localization superresolution microscope. Data volumes are displayed in point splatting view. **(G)** Representative segmentation of juxta-nuclear clump versus the rest of the cells as used for the STORM analysis. Note that the image used to indicate the segmentation in G is identical to the image used to represent the localization SSTR2 and syntaxin-6 in A. **(H)** The spatially unrelated Giantin and PIST single-molecule localizations are used as a negative control for the distance analysis. Scale bars represent 5 µm.

SSTR2 GLSVs are mobilized in response to CRF in a Rab10-dependent manner

Rab GTPases are critical switches in membrane trafficking controlling nearly all aspects of vesicle formation, transport, and docking/fusion (Aloisi and Bucci, 2013). In addition to Rab10, both Rab8 and Rab13 have been shown to be involved in trafficking of GSVs in myocytes (Sun et al., 2010, 2016). We thus transfected HeLa cells with mCherry-tagged Rab8, Rab10, and Rab13 and EGFP-SSTR2. Whereas Rab8 and Rab13 displayed little colocalization with internalized SSTR2 (Fig. 8 A and Videos 7 and 8), Rab10 displayed robust colocalization and was seen to cotraffic with SSTR2 (Fig. 8 A and Video 9). This is consistent with the observation that Rab10 is present on syntaxin-6–positive structures immunoisolated from cell lysates (Fig. 5).

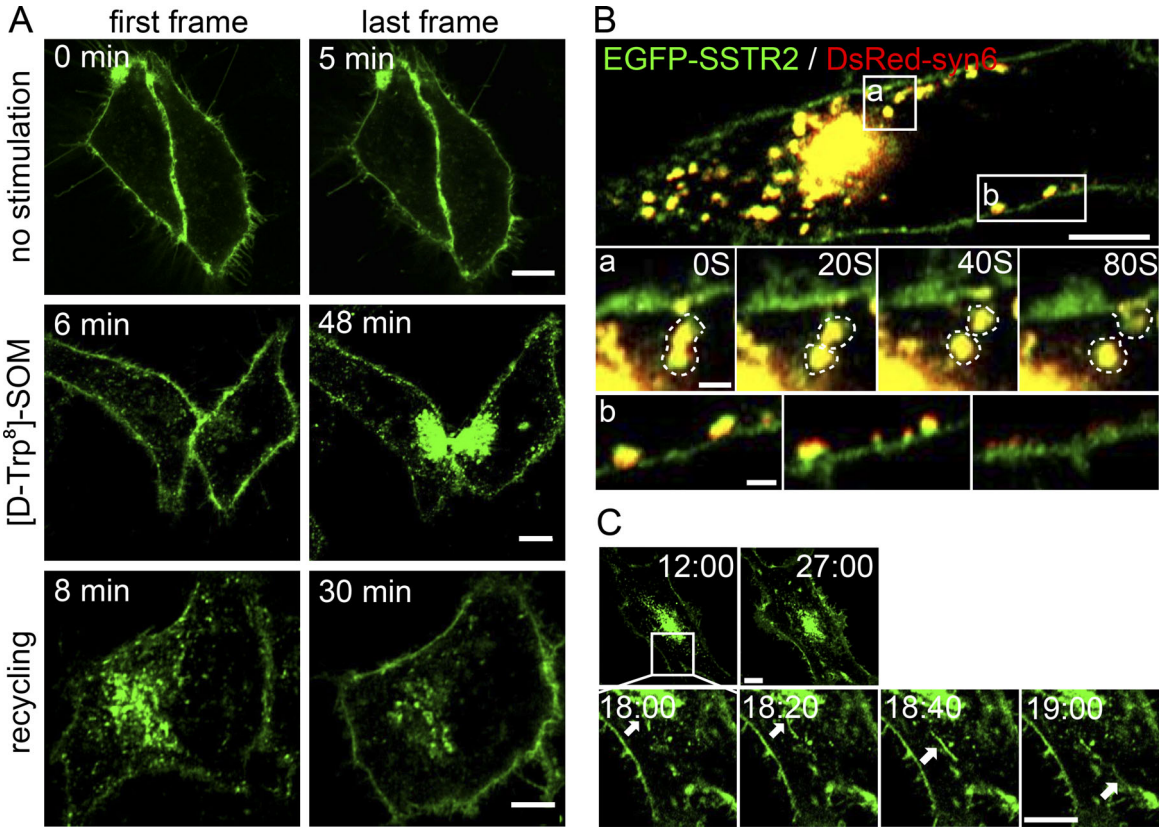

Figure 7. **Dynamics of SSTR2 trafficking. (A)** HeLa cells transfected with EGFP-SSTR2 were imaged for 5 min in the absence of stimulation (top two panels), for 42 min 6 min after applying [D-Trp^8]-SOM (middle two panels), or for 22 min 8 min after agonist washout (bottom two panels). The images are the first and last frames from Videos 1, 2, and 3, respectively. **(B)** HeLa cells were transfected with EGFP-SSTR2 and Ds-Red-syntaxin-6. Cells were incubated for 60 min with 100 nM of [D-Trp^8]-SOM followed by brief acid wash, and the cells were then imaged using a Zeiss LSM 880 microscope with airyscan at 10- to 20-s intervals. The images represent frames from Videos 4 and 5. The boxed areas in the top panel are shown at higher magnification below. The dashed lines in B indicate SSTR2/syntaxin-6–positive vesicles. Scale bars in A and B represent 5 µm and 1 µm for the low- and high-magnification images, respectively. **(C)** HeLa cells were transfected with EGFP-SSTR2 and imaged live following 60 min of [D-Trp^8]-SOM incubation and a brief acid wash. Representative cropped frames from Video 6 are shown. The arrows indicate SSTR2 transport on a tubular carrier. Scale bar represents 5 µm.

Interestingly, the Rab10/SSTR2 vesicles reach the cell surface followed by transfer of SSTR2 into the plasma membrane (Fig. 8 A and Video 10).

To determine if Rab10 is involved in SSTR2 surfacing, we used CRISPR/Cas9 to generate two Rab10 knockout AtT20 cell lines. In both lines, Rab10 was depleted to levels undetectable by immunoblot (Fig. 8 B). There were no obvious compensatory changes in the levels of the evolutionarily related Rab8 and Rab13 or in levels of Rab5 or Rab35, both of which have endosomal functions (Fig. 8 B). We then used immunofluorescence to examine the localization of SSTR2 in the knockout cells compared with wild-type AtT20 cells and an isogenic control line that underwent the same CRISPR-based procedure without Rab10 knockout. In Rab10 knockout cells, as in the control lines, SSTR2 was localized predominantly to the plasma membrane at the basal level, and stimulation with [D-Trp^8]-SOM for 60 min induced SSTR2 internalization, resulting in a comparable reduction in surface levels (Fig. 8, C and D). After 1-h recycling, SSTR2 plasma membrane levels were increased to 47% in the wild-type cells and 39% in the isogenic control cells. This increase was reduced to 31% and 22% in the two Rab10 knockout lines, although the decrease was not significant (Fig. 8 D). Thus, Rab10 appears to have a limited role in the basal recycling of internalized SSTR2.

We next sought to examine if GLSVs carrying SSTR2 could be mobilized in response to selective signals. CRF activates the CRF receptor to stimulate ACTH secretion from corticotropes, including AtT20 cells. We thus hypothesized that CRF receptor activation could drive surfacing of SSTR2 as a negative feedback mechanism to regulate CRF action. We treated AtT20 cells for 60 min with [D-Trp^8]-SOM to induce maximal SSTR2 internalization followed by incubation in serum-free culture media for 1 h at 37°C, with or without 100 nM CRF. [D-Trp^8]-SOM stimulation resulted in a 77.2% loss of SSTR2 cell surface levels (Fig. 9, A and B). Recycling for 1 h under basal conditions resulted in a 20.5% increase in SSTR2 surface levels, but remarkably, in the presence of CRF, this number rose to 64.0%, a highly significant ($P < 0.001$) 43.5% increase as compared with 1-h recycling in the absence of CRF (Fig. 9, A and B). Thus, CRF mobilizes SSTR2 from an intracellular pool to the cell surface, and given that SSTR2 activation attenuates CRF signaling (Litvin et al., 1986; Richardson and Schonbrunn, 1981), this membrane trafficking process could potentially provide a feedback mechanism to control ACTH release (Fig. 9 E).

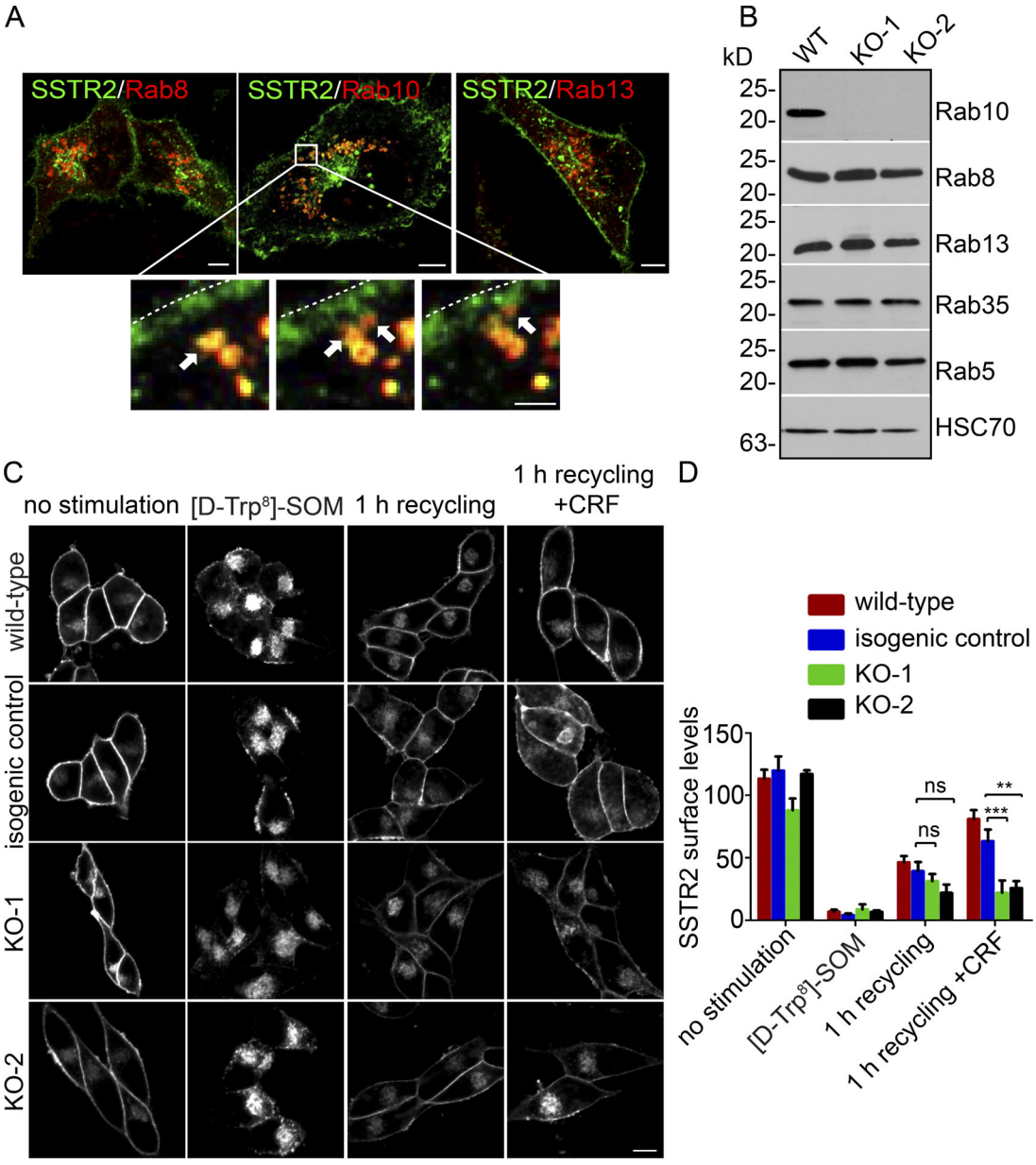

Figure 8. **Rab10 is involved in SSTR2 recycling. (A)** HeLa cells expressing EGFP-SSTR2 along with mCherry-Rab8, mCherry-Rab10, or mCherry-Rab13 were imaged live, with the figure revealing cropped frames from Videos 7–9. The boxed area from the Rab10-transfected cells is shown at higher magnification below. Arrows indicate SSTR2/Rab10-positive vesicles moving toward and fusing with the plasma membrane, which is indicated by the dashed line. Scale bars represent 5 µm and 1 µm for the low- and high-magnification images, respectively. **(B)** Representative immunoblots from wild-type (WT) AtT20 cells and two Rab10-knockout (KO) cell lines generated using CRISPR/Cas9. The migration of molecular weight markers in kilodaltons is indicated. **(C)** AtT20 cells, either wild-type, two Rab10 knockout lines (KO-1 and KO-2), and an isogenic control were left untreated (no stimulation) or were treated for 60 min with [D-Trp^8]-SOM to induce maximal SSTR2 internalization, followed by a brief acid wash and incubation in ligand-free media for 1 h at 37°C, without or with 100 nM CRF. Following the treatments, cells were fixed and processed for immunofluorescence with antibody recognizing SSTR2. Scale bar represents 5 µm. **(D)** Quantification of SSTR2 cell surface immunofluorescence intensity of three successive experiments as in C. Data were analyzed by two-way ANOVA and Bonferroni comparison test (procedures implemented in GraphPad statistical package). Data are presented as least-square means ± SEMs with treatment effects significant at 0.05. **, $P \le 0.01$; ***, $P \le 0.001$.

Stimulation of the CRF receptor leads to an increase in cytosolic Ca^{2+} and cAMP levels (Litvin et al., 1986; Tojo and Abou-Samra, 1993). Conversely, activation of either SSTR2 or SSTR5 inhibits L-type calcium channels (Tallent et al., 1996) and reduces cAMP (Strowski et al., 2002) necessary for regulated hormone secretion in AtT20 cells. We thus sought to test if direct activation of these signaling pathways also mobilizes GLSVs. We thus used SOM to drive SSTR2 internalization and subsequently treated the cells with Bay K8644, an agonist of voltage-gated Ca^{2+} channels (Reisine, 1990), or a combination of forskolin and 3-isobutyl-1-methylxanthine (IBMX), which increases cAMP levels (Tojo and Abou-Samra, 1993). Both led to significant increases in SSTR2 surface levels after 1-h treatment as compared with 1-h recycling in the absence of the drugs (Fig. 9, A and B).

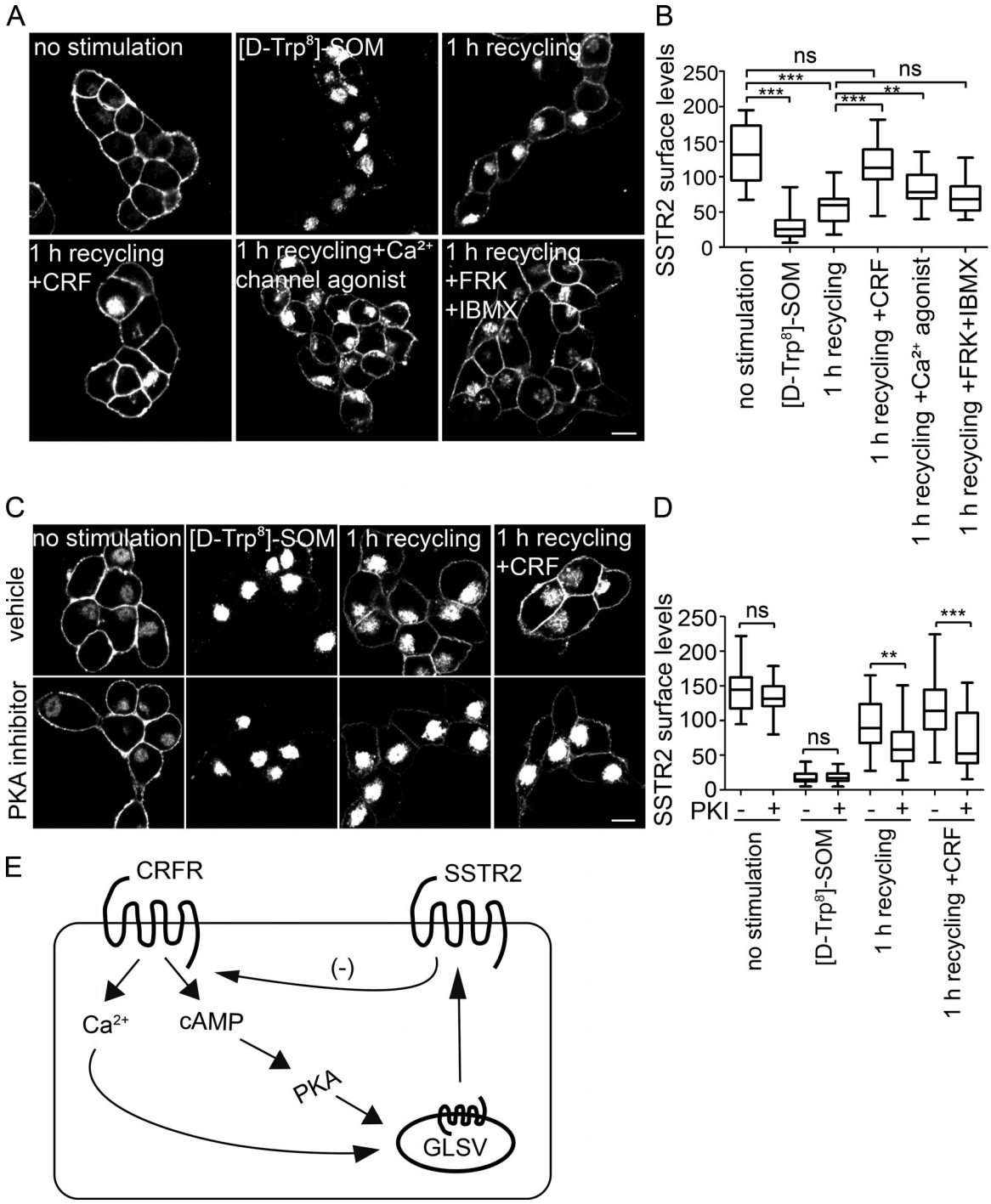

Figure 9. **SSTR2 recycling is enhanced in response to physiological signals. (A)** AtT20 cells were treated for 60 min with [D-Trp^8]-SOM to induce maximal SSTR2 internalization followed by brief acid wash and incubation in ligand-free media for 1 h at 37°C without or with 100 nM CRF, 50 nM Bay K8644, a Ca^{2+} channel agonist, or 10 µM forskolin/1 mM IBMX. Following the treatments, cells were fixed and processed for immunofluorescence with antibody recognizing SSTR2. Scale bar represents 10 µm. **(B)** Quantification of SSTR2 cell surface immunofluorescence intensity of three successive experiments as in A. Data were analyzed by one-factor ANOVA and Tukey comparison test (procedures implemented in GraphPad statistical package). Data are presented as least-square means ± SEMs with treatment effects significant at 0.05. **(C)** AtT20 cells were treated for 60 min with [D-Trp^8]-SOM with or without 10 µM PKI followed by brief acid wash and incubation in ligand-free media for 1 h at 37°C without or with 100 nM CRF and PKI. Following the treatments, cells were fixed and processed for immunofluorescence with antibody recognizing SSTR2. Scale bar represents 10 µm. **(D)** Quantification of SSTR2 cell surface immunofluorescence intensity of two successive experiments as in C. Data were analyzed by one-factor ANOVA and Tukey comparison test (procedures implemented in GraphPad statistical package). **, $P \leq 0.01$; ***, $P \leq 0.001$. **(E)** Cartoon model for the induced SSTR2 recycling from the GLSV compartment. Following internalization after SOM binding, SSTR2 is sequestered in a GLUT4 like storage vesicles in endocrine cells. The recycling dynamics is very slow and can be stimulated by activation of CRF receptor (CRFR) or activation of its downstream signaling pathways.

Additionally, direct inhibition of protein kinase A activity using the cell-permeable myristoylated protein kinase A inhibitor (PKI) 14–22 amide (Glass et al., 1989) decreased the cell surface levels of SSTR2 by 37.3% ($P < 0.005$) and 46.7% ($P < 0.001$) as compared with 1-h recycling in the absence or presence of CRF, respectively (Fig. 9, C and D). Thus, the GLSVs containing SSTR2 can be mobilized in response to physiological ligands, similar to the GSVs that carry GLUT4 (Fig. 9 E).

We then reexamined SSTR2 recycling in Rab10 knockout cells. CRF treatment of the isogenic control cells during the 1-h recycling window led to an increase in plasma membrane levels of SSTR2 to 63.3% of untreated cells. Remarkably, this increase was significantly blunted to 22.0% and 26.0% in the two Rab10 knockout cell lines (Fig. 8, C and D). Consistently, the CRF effect was restored when Rab10 was transfected in the two Rab10 knockout cells lines (Fig. S3 A). Thus, CRF mobilizes GLSVs, bringing SSTR2 to the cell surface in a Rab10-dependent manner. Furthermore, upon transfection into AtT20 cells, GLUT4 is sorted to the same structures that contain internalized SSTR2 and syntaxin-6 (Fig. S3 B). Taken together, these data indicate that SSTR2 is localized to GLSVs that are physiological analogues of GSVs.

Regulation of SSTR2 resurfacing in mouse somatotropes in vivo

SOM is a negative regulator of hormone secretion from all pituitary cell types. It has been hypothesized that SOM may help shape rhythms of hormone secretion driven by the stimulatory releasing hormones by also undergoing pulsatile release from the hypothalamus, but this is hard to reconcile with the fact that hormone release from the various cell types displays unique patterns. The finding that the recycling of SSTR2 to the plasma membrane is enhanced by the activation of a coexpressed stimulatory receptor led us to hypothesize that such trafficking-based mechanisms may fine-tune the regulation of pituitary secretions in vivo. To test this hypothesis, we used the pituitary GH system that has a recognizable and well-studied pattern of secretion in male rodents (Steyn and Ngo, 2017; Stroh et al., 2009; Tannenbaum, 1993; Tannenbaum et al., 1990, 1993). We tracked the GH secretion profiles of 11 mice, which displayed typical pulsatile patterns of blood GH with high-amplitude sharp GH apexes (4–20 ng/ml) interrupted by periods of very low or undetectable basal plasma GH levels (nadir; Fig. 10 C). Based on these profiles, we caught six mice during the blood GH nadir periods (mice 1–6), two mice in the declining phase of the apex period (mice 7 and 8), and three mice in the ascending phase of the apex period (mice 9–11; Fig. 10 C). To examine the cellular distribution of SSTR2 in pituitary somatotropes to test for potential correlations with the different phases of the GH release cycle, we stained 4-µm sections of pituitary gland for SSTR2 and GH. The maximal fluorescent signal was obtained when sections were individually stained for SSTR2 and GH on consecutive sections. In this case, somatotrope-rich areas were identified, and the same area on the SSTR2-labeled section was imaged. Examples of double labeling of SSTR2 and GH on the same sections is also demonstrated (Fig. S4 D). We observed that the SSTR2 immunoreactive signal was distributed between the plasma membrane and cytoplasmic stores depending on the phase of the GH cycle (Fig. 10 A and Fig. S4, A–D). Quantification of SSTR2 reveals that the average ratio of the plasma membrane to intracellular signal is 1.0 at the nadir (Fig. 10 B). During the apex of blood GH, the plasma membrane to intracellular ratio of SSTR2 reaches between 1.5 and 2.2, with an average of 1.7 (Fig. S4, B and C). Thus, there is a correlation between the subcellular localization of SSTR2 with the different phases of blood GH. The presence of SSTR2 at the plasma membrane during the GH blood apex is consistent with the enhanced recycling observed upon the activation of the hormone secretion stimulating receptor in corticotropes.

Discussion

Understanding the trafficking itinerary of a signaling receptor can provide valuable information into the regulation of its function, with insight into cellular and physiological behaviors. It was previously reported that after endocytosis, SSTR2, a major regulatory signaling GPCR in the pituitary, is transported to a juxtanuclear syntaxin-6–positive compartment with the interpretation that the receptor is brought to the TGN (Csaba et al., 2007). Here, we confirm the localization of internalized SSTR2 with syntaxin-6 but provide compelling evidence that syntaxin-6 is not a marker of the TGN. Syntaxin-6 is a soluble N-ethylmaleimide attachment protein receptor that mediates membrane fusion (Bock et al., 1996). In this way, it fulfills versatile functions in vesicle exocytosis depending on the cell type (Jung et al., 2012; Wendler and Tooze, 2001), and thus, its cellular localization is reflective of its role. An early single-labeling electron microscopy study localized syntaxin-6 mainly to the TGN and adjacent vesicles in PC12 cells (Bock et al., 1997). Ever since, syntaxin-6 has been widely used as a TGN marker. Since the TGN shows a complex arrangement of tubular/vesicular membranes, it is hard to structurally discriminate in single staining electron microscopy. Here, double-labeling immunocytochemical experiments, analyzed with standard and super-resolution confocal microscopy, and biochemical fractionation studies reveal that most syntaxin-6 does not colocalize with the TGN-resident proteins PIST and TGN38. Moreover, Brefeldin A treatment was able to functionally dissect syntaxin-6–enriched structures from the TGN. The fungal metabolite Brefeldin A inhibits anterograde protein transport from the endoplasmic reticulum to the Golgi by blocking the recruitment of COPI coats (Cole et al., 1996). The loss of COPI causes the Golgi cisternae to fuse with the endoplasmic reticulum (Hess et al., 2000) and the TGN to tubulate into the cytoplasm and fuse with endosomes (Reaves and Banting, 1992; Wood et al., 1991). While Brefeldin A causes TGN38 and PIST immunoreactivity to disperse into punctate signals throughout the cytoplasm, consistent with previous reports for TGN resident proteins (Chege and Pfeffer, 1990; Lippincott-Schwartz et al., 1991; Reaves and Banting, 1992; Tooze and Hollinshead, 1992; Wagner et al., 1994), SSTR2 as well as syntaxin-6 fluorescent signals remain intact as a juxtanuclear concentration. This is seen in multiple cell types, including primary cultures of neurons. Together, these findings demonstrate that syntaxin-6 defines a functionally distinct TGN

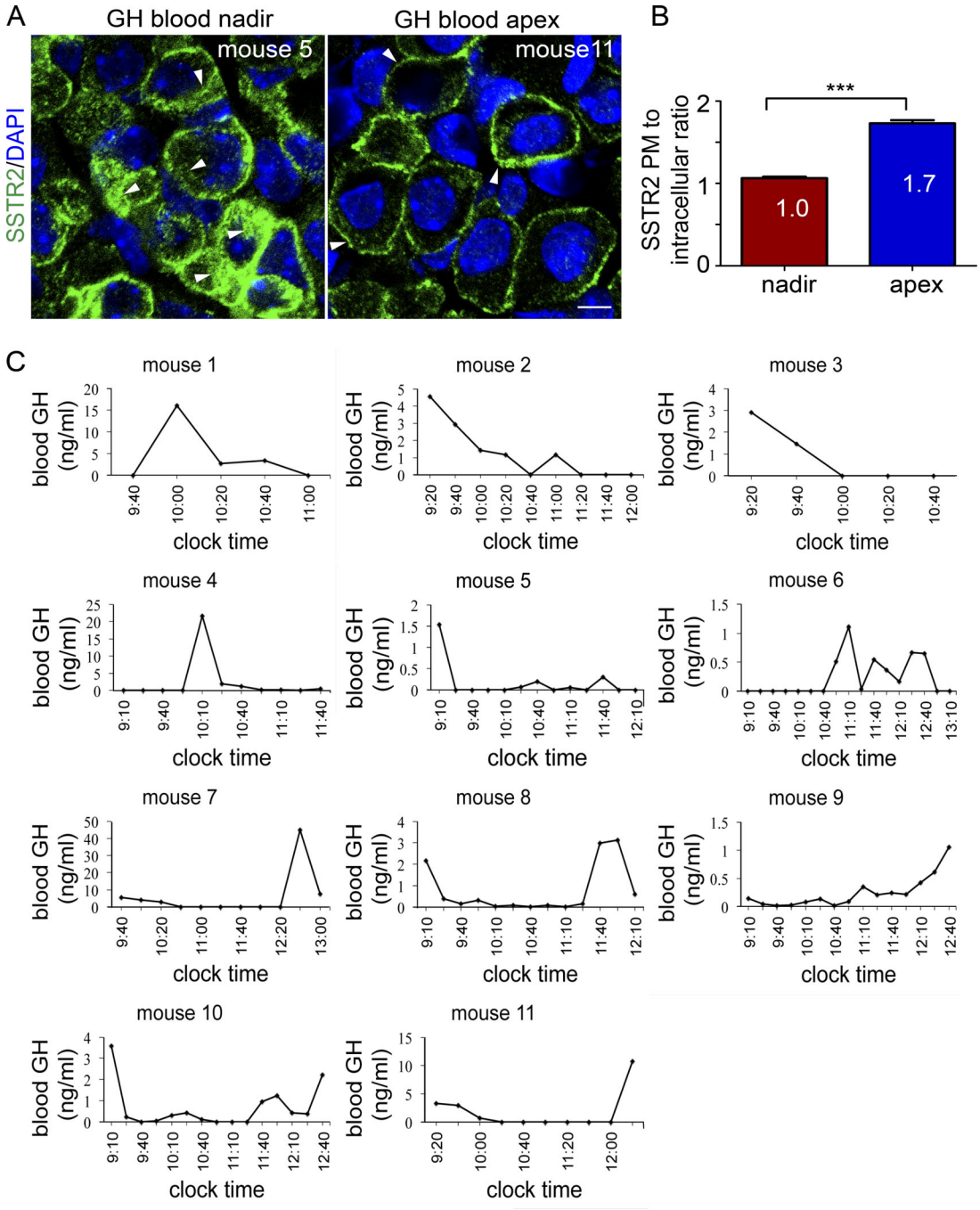

Figure 10. **Coronal sections through the mice anterior pituitary gland immunostained for SSTR2. (A)** Coronal sections through the anterior pituitary of mouse 5, which was at a GH blood nadir at time of sacrifice, and mouse 11, which was at a GH blood apex at time of sacrifice. The sections are stained with antibody recognizing SSTR2 and with DAPI to reveal nuclei. Arrowheads point to predominantly intracellular staining in mouse 5 and cell surface staining in mouse 11. Scale bar represents 25 µm. **(B)** Average SSTR2 immunoreactive signal presented as ratio of plasma membrane to cytoplasmic signals from mice grouped depending on the GH status. Data were analyzed by Student's *t* test in GraphPad prism 5. Data are presented as least-square means ± SEMs with treatment effects significant at $P < 0.05$. ***, $P \leq 0.001$. **(C)** Blood samples (2 µl) were collected from the tip of the tails at least 2 h before the sacrifice time at 15- to 20-min intervals. The level of GH in blood was measured using a sensitive sandwich ELISA.

adjacent cellular compartment that in pituitary cells receives internalized SSTR2.

While syntaxin-6 has been thought of as a TGN marker, other studies describe it as defining a specialized storage and recycling compartment for GLUT4 in adipocytes (Shewan et al., 2003) and muscle cells (Foley and Klip, 2014). The insulin-responsive syntaxin-6–positive GSVs are structurally segregated from both endosomes and the TGN (Foley and Klip, 2014; Martin et al., 1994). Here, we describe a similar subcompartment in AtT20 pituitary endocrine cells that we have termed GLSVs. We find that Rab10, a functional marker that mediates GSV exocytosis, spatially and functionally associates with SSTR2-positive GLSVs

during exocytosis. The recycling of the GLSVs is relatively slow, and thus, the receptors are stored with a half-life of ∼4 h. Moreover, like GSVs, the GLSVs are mobilized by a physiological ligand, CRF, and signaling components downstream of the CRF receptor. In this context, it is interesting that the recycling of SSTR2 has much faster kinetics in HeLa cells than in AtT20 cells, suggesting that there are factors in AtT20 cells that constrain recycling that are absent in HeLa cells, which lack endogenous SSTR2. One possibility is the lack of the protease necessary for liberating the GLSVs from intracellular sequestration in HeLa cells. Another possibility is the differential expression and/or differential activity of endosomal peptidases such as endothelin-converting enzyme-1 that was shown to be necessary for ligand degradation and liberation of SSTR2 for recycling (Zhao et al., 2013).

This study thus demonstrates that the concept of a physiological mobilizable storage compartment needs to be expanded beyond GLUT4 in muscle and fat cells. In fact, there already appears to be several such specialized vesicles. For example, the aquaporin 2 water channel is stored intracellularly and mobilized to the apical membrane of kidney ductal cells in response to vasopressin signaling (Park and Kwon, 2015). Similarly, the AMPA receptor is stored inside the postsynaptic compartment and is mobilized to the synaptic plasma membrane in response to paired polarization of pre- and postsynaptic neurons to potentiate synapses (Choquet, 2010). It is well established that signaling and trafficking of GPCRs are highly intertwined in that receptor localization can shape receptor signaling capacities and the trafficking of GPCRs can be regulated by extracellular signals that impinge on the receptors (Sorkin and von Zastrow, 2009). For example, in the latter regard, substance P activation of the neurokinin 1 receptor enhances the μ-opioid receptor after endocytic recycling in a protein kinase C–dependent manner (Bowman et al., 2015). Protein kinase A–mediated phosphorylation of the β2-adrenergic receptor ensures its recruitment to the sequence-dependent recycling microdomain on endosomes allowing for slower regulated recycling (Vistein and Puthenveedu, 2013). Therefore, while the observation that activation of the CRF receptor leads to enhanced recycling of SSTR2 is simply another example of regulation of GPCR trafficking, it is unique in that it involves mobilization of a GLSV.

We asked whether the feedback mechanism observed in corticotropes between the hormone release stimulating CRF receptor and the hormone release inhibiting SSTR2 could provide a mechanism to fine-tune endogenous rhythms of pituitary hormone release. We tested this hypothesis in the well-studied GH system because of its sharp and consistent ultradian rhythm of GH release. In male rodents, pituitary somatotropes have secretory GH bursts (apex) with intervening trough periods where plasma GH levels are undetectable (nadir). While it is clear that SOM and GHRH each play crucial roles in GH regulation, current theories only discuss an interaction between SOM and GHRH at the level of their release. It is well understood that SOM antagonizes GH release, leading to a hypothetical model where the pulsitility of GH secretion is established by a temporal reciprocal release of GHRH and SOM. According to this model, a pulse of GHRH release from the hypothalamus will lead to a peak of GH release, followed by a pulse of SOM, which leads to the nadir of GH release (Frohman et al., 1990; Soya and Suzuki, 1988; Soya et al., 1990; Stachura et al., 1988; Tannenbaum and Ling, 1984). There is strong evidence that peaks of GH secretion are due to preceding pulses of GHRH. Animals bearing lesions of the ventromedial-arcuate region of the hypothalamus exhibit a marked suppression in amplitude of GH secretory bursts (Eikelboom and Tannenbaum, 1983; Martin et al., 1974; Tannenbaum et al., 1983), which is restored by the administration of GHRH (Tannenbaum et al., 1983). Furthermore, immunoneutralization with a monoclonal antibody specific for rat hypothalamic GHRH abolishes the GH pulses (Wehrenberg et al., 1982). Moreover, direct measurement of GHRH and SOM in the portal blood from sheep (Frohman et al., 1990) established a significant association between GHRH pulses in the portal blood and GH secretory peaks. However, the study found no significant association between SOM levels in the portal blood and the GHRH or GH nadir. Moreover, if endogenous SOM levels are high only during periods of low plasma GH levels, injecting SOM neutralizing antiserum should elevate basal GH levels during the nadir periods but has no effect on the GH peaks. However, the effect of SOM antiserum on the amplitude of GH peaks ranged from an increase (Ferland et al., 1976; Varner et al., 1980) to a decrease (Steiner et al., 1978) to no significant change (Terry and Martin, 1981). Additionally, basing the regulation of GH solely on the timing of SOM release might not be sound, because SOM is involved in the regulation of other pituitary hormones with different secretion patterns (den Boon and Sarabdjitsingh, 2017; Durán-Pastén and Fiordelisio, 2013; Steyn and Ngo, 2017). Thus, we believe that another layer of regulation, at the level of the receptors, is what gives specificity for individual hormone regulation by SOM. According to our hypothesis, GHRH binds to the GHRH receptor on pituitary somatotropes, activating GH release through increasing cytosolic cAMP and Ca^{2+} levels and leading to a GH peak in blood. Simultaneously, GHRH receptor activation stimulates SSTR2 resurfacing in GLSVs. Once at the surface, SSTR2 binding to SOM activates inhibitory G protein signaling, reducing cytosolic cAMP and Ca^{2+} levels and stopping GH secretion. This is followed by internalization and sequestration of SSTR2 in GLSVs until another pulse of GHRH, when the cycle starts over. Overall, we propose SSTR2 trafficking as a regulatory mechanism contributing to the fine-tuning of the endogenous rhythms of the different pituitary hormones, exerting a previously unrecognized mechanism to ensure the specificity of regulation in a cell type–specific manner.

Materials and methods

Peptides, drugs, and antibodies

[D-Trp^8]-SOM, CRF (catalog number C3042), forskolin (catalog number F3917), IBMX (catalog number I5879), dynasore hydrate (catalog number 7693), cycloheximide (catalog number c7698), Bay K8644 (catalog number B112), and the cell-permeable PKI 14–22 mristoylated amide (catalog number 476485) were purchased from Sigma-Aldrich. The DyLight 488 Conjugation Kit was purchased from Abcam (catalog number ab201799). The

various antibodies used in this study were from the indicated sources and were validated for specificity in the indicated references: polyclonal guinea-pig anti-PIST (1:10,000; custom immunization by Biogenes; validated in Fig. S5 B); polyclonal rabbit anti-TGN38 (catalog number AHP1597; AbD Serotec; Luzio et al., 1990); monoclonal mouse anti-Giantin antibody (catalog number ALX-804-600-C100; Enzo Life Sciences). The rabbit polyclonal GH antibody (catalog number ab126882), mouse monoclonal anti-Rab10 antibody (catalog number ab104859; validated in Fig. 8 B), rabbit polyclonal anti-Rab 5 (catalog number ab18211), monoclonal rabbit anti-PIST antibody (catalog number ab109119), and monoclonal rabbit anti-SSTR2 (catalog number ab134152; Fischer et al., 2008) were purchased from Abcam. Mouse anti-syntaxin-6 (catalog number 610635) was purchased from BD Transduction Laboratories (validated in Fig. S5 A). Monoclonal rabbit anti-Rab8 (D22D8) was purchased from Cell Signaling Technology; polyclonal anti-Rab35 was raised in rabbit against GST-tagged full-length human Rab35 (Allaire et al., 2010), and rat monoclonal anti-HSC70 antibody was purchased from Enzo Life Sciences. Alexa Fluor 647–conjugated Trf (catalog number T23366), Alexa Fluor 647–conjugated goat anti-guinea pig (catalog number A-21450), and Alexa Fluor 488–conjugated goat anti-rabbit secondary antibodies (catalog number A-11008) were purchased from Life Technology. Cy3-conjugated goat anti-rabbit (catalog number 111–165-144) and Cy3-conjugated goat anti-mouse (catalog number 115–165-146) were purchased from Jackson ImmunoResearch Laboratories. Goat anti-guinea pig star red (catalog number 2–0112-011-8) and goat anti-mouse star red (catalog number 2–0002-011-2) were purchased from Abberior. Goat anti-rabbit CF568 (catalog number 2102) was purchased from Biotium.

Plasmids

A construct encoding full-length human SSTR2 in pMD18-T cloning vector (catalog number HG11644-M; Sino Biological) was inserted into pEGFP-C3 plasmid coding for a signal peptide (peptide sequence: mvlwlqlallalllptslaqgevdi; a gift from Dr. Hans-Jurgen Kreienkamp, Universitätsklinikum, Freiburg, Germany), using forward primer 5′-ATATATAAGCTTATGGAC ATGGCGGATGAGCCACTC-3′ and reverse primer 5′-ACTACT CTCGAGTCAGATACTGGTTTGGAGGTCTCC-3′. The full-length human syntaxin-6 in a pDsRedC1 vector was a gift from Dr. Mien-Chie Hung (University of Texas, Houston, TX). Full-length wild-type human Rab8, cloned into pCherry between the Kpn1 and BamH1 sites, was a gift from Dr. Elena Torban (McGill University, Montreal, Canada). The gene encoding full-length wild-type rat Rab10 in pmCherry-C3 was a gift from Dr. Marc McNiven (Mayo Clinic, Rochester, MN). MCherry-tagged human wild-type Rab13 was inserted in pmCherry-C3 (Ioannou et al., 2016). EGFP-Rab10Q68L (#49544), pLenti-myc-GLUT4-mCherry (#64049), and pB-GLUT4-7myc-GFP (#52872) were all purchased from Addgene.

For transfection of EGFP-Rab10Q68L in AtT20 cells, 100,000 cells of the isogenic AtT20 control or the two Rab10 knockout lines were suspended in 300 µl electrolytic buffer (Invitrogen) containing 5 µg EGFP-Rab10Q68L and transferred to a 0.4-mm electroporation cuvette. Electroporation was performed using Bio-Rad Gene Pulser X with two pulses of 20 ms each at 200 V with a square wave setting. Cells were then immediately plated onto poly-L-lysine–coated glass coverslips (Nunc) in four-well plates containing culture media prewarmed to room temperature. Cells were incubated at 37°C for 72 h before the start of the experiment. Similarly, GLUT4-mCherry or GLUT4-GFP were electroporated into AtT20 cells and incubated for 24 h before the start of the experiment. Preliminary experiments were performed to optimize the electroporation parameters until a 15–20% transfection efficiency was achieved.

Cell seeding

For each staining experiment, ∼100,000 AtT20 cells were plated on poly-L-lysine–coated glass coverslips (Nunc) in four-well plates or on glass-bottom wells from 8-well chamber slides (Nunc) for STORM imaging or in 35-mm glass-bottom MatTek dishes for time-lapse imaging. Cells were plated in DMEM for 24 h in a 37°C, 95% air + 5% CO_2 incubator. Just before the start of the experiment, the cells were equilibrated for 10 min at 37°C in open room atmosphere in Earle's buffer (pH 7.4) containing 2% BSA and 0.1% D-glucose. Pharmacological agents were added to the Earle's buffer in experiments requiring them.

Internalization of SSTR2 and Trf

AtT20 cells were serum-starved for 2 h in a serum-free DMEM to deplete natural Trf before they were equilibrated in Earle's buffer. The equilibrium buffer was replaced by Earle's buffer containing Alexa Fluor 647–conjugated Trf (5 µg/ml), along with 100 nM of [D-Trp^8]-SOM 40 min on ice for the 0-min stimulation point or at 37°C for the 5- and 40-min stimulation point. Ice-cold Earle's buffer was used to end the stimulation. Cells were then fixed in 4% PFA followed by immunofluorescence labeling for SSTR2 using the monoclonal rabbit anti-SSTR2 and Alexa Fluor 488–conjugated goat anti-rabbit and for syntaxin-6 using the mouse monoclonal anti-syntaxin-6 antibody and Cy3-conjugated goat anti-mouse secondary antibodies. Cells were imaged using LSM 710 confocal microscope as single optical section.

Brefeldin A treatment

Brefeldin A (10 µM) or DMSO were added to the cells in Earle's buffer 15 min before and during the 40-min stimulation with 100 nM of [D-Trp^8]-SOM at 37°C. The stimulation was ended by ice-cold Earle's buffer, and the cells were processed for immunofluorescence labeling.

Nocodazole treatment

Nocodazole (20 µg/ml) or DMSO was added directly to the DMEM for 2 h. The media was then replaced with 10 min of Earle's buffer for equilibration followed by 40 min of [D-Trp^8]-SOM stimulation with or without nocodazole. The stimulation was ended by ice-cold Earle's buffer, and the cells were processed for immunofluorescence labeling.

Dynasore treatment

Cells were washed five times with Earle's buffer to remove any traces of serum albumin. Dynasore (80 µM) or DMSO was added

to the cells in Earle's buffer 20 min before and during the 40-min stimulation with 100 nM [D-Trp^8]-SOM at 37°C. The stimulation was ended by ice-cold Earle's buffer, and the cells were processed for immunofluorescence labeling.

Sucrose treatment

Sucrose (0.45 M) was added to cells in Earle's buffer and incubated for 15 min before and during the 40-min stimulation with 100 nM of [D-Trp^8]-SOM at 37°C. The stimulation was ended by ice-cold Earle's buffer, and the cells were processed for immunofluorescence labeling.

Cycloheximide treatment

Cycloheximide (100 µg/ml) or DMSO were added to cells 2 h before and during the 40-min stimulation with 100 nM of [D-Trp^8]-SOM at 37°C. The stimulation was ended by ice-cold Earle's buffer, and the cells were processed for immunofluorescence labeling.

PKI 14–22 treatment

The cell-permeable PKI 14–22 mristoylated amide (10 µM) was added to the cells in Earle's buffer during the 40-min stimulation with 100 nM [D-Trp^8]-SOM at 37°C. The stimulation was ended by ice-cold Earle's buffer, and the cells were processed for the SSTR2 recycling assay followed by immunofluorescence labeling for SSTR2. When PKI was used, it was maintained throughout the length of stimulation.

SSTR2 recycling assays

Cells were seeded and equilibrated as described. This was followed by 40 min of stimulation with 100 nM [D-Trp^8]-SOM. The cells were then washed briefly with hypertonic acid wash (Earle's buffer containing 0.2 M acetic acid and 0.5 M NaCl, pH 4) to remove surface attached ligand (Nouel et al., 1997; Stroh et al., 2000). Immediately, the acid wash was replaced with 37°C warm DMEM and maintained at 37°C in a humidified atmosphere of 95% air and 5% CO_2 for 1, 4, or 24 h for Fig. 2 and Fig. S1 or for 1 h in serum-free DMEM with or without 100 nM CRF, 10 µM forskolin/1 mM IBMX, or 50 nM Bay K86449 for Fig. 8 C and Fig. 9 (A and C) before fixation and immunofluorescence labeling for SSTR2.

Immunofluorescence

Cells were fixed with 4% PFA for 20 min followed by blocking/permeabilization for 15 min in TBS containing 5% normal goat serum (NGS; Jackson ImmunoResearch Laboratories), 2% BSA, and 0.05% saponin. Immunolabeling was performed by incubating cells overnight at 4°C with appropriately diluted primary antibodies in TBS containing 0.05% saponin and 1% NGS. Subsequently, the cells were washed in TBS and incubated for 40 min at room temperature with the appropriate species-specific secondary antibodies conjugated to Alexa Fluor 647, Alexa Fluor 488, or Cy3 and diluted in TBS containing 0.05% saponin and 1% NGS. Cells were then washed with TBS and mounted with Aqua poly mount (#18606; Polysciences) for confocal imaging or prolong gold anti-fade reagent (Invitrogen) for STED imaging onto glass slides.

Time-lapse imaging

HeLa cells were transfected 48 h before imaging with 2 µg plasmid DNA for EGFP-SSTR2 along with mCherry-Rab10, mCherry-Rab8, mCherry-Rab13, or DsRed-syntaxin-6. Images were obtained using the fast airyscan of Zeiss LSM 880 microscope with a 37°C incubation chamber and Plan-Apo 63×/NA 1.40 oil objective. After [D-Trp^8]-SOM stimulation for 60 min, cells were quickly acid washed and imaged in Earle's buffer for the times indicated on the images at 10- to 20-s intervals.

Optical nanoscopy

Cells were stimulated with 100 nM [D-Trp^8]-SOM for 60 min before fixation and standard immunolabeling for SSTR2 using the anti-SSTR2 (1:5,000), for syntaxin-6 using the mouse monoclonal anti-syntaxin-6 antibody (1:500), or for PIST using the guinea pig anti-PIST antibody (1:5,000). Labeling was visualized using Alexa Fluor 647–conjugated goat anti-mouse (1:1,000) and goat anti-rabbit CF568 (1:1,000) or the Alexa Fluor 647–conjugated goat anti-guinea pig (1:1,000). Images were acquired in imaging buffer (50 mM Tris-HCl, 10 mM NaCl, and 10% [wt/vol] glucose, pH 8) containing 20 mM MEA, 1% (vol/vol) 2-mercaptoethanol (Sigma-Aldrich), a168.8 a.u. glucose oxidase (Sigma-Aldrich), and 1,404 a.u. catalase (Sigma-Aldrich). The cells were imaged using Vutara SRX-350 STORM microscope using a 60×, Olympus Plan-Apo water-immersion (NA 1.20) and Hamamatsu sCMOS camera at 50 frames per second. Fluorophores were activated with a 405-nm diode laser at 40 mW and imaged sequentially with a 561-nm laser at 300 mW and a 640-nm laser at 315 mW. 3D dSTORM superresolution data of 8,000 frames was reconstructed and the nearest-neighbor analysis of the region of interest (ROI), as shown in Fig. 6 G, was done using Vutara SRX 6.04.02 software with the colocalization function.

STED imaging

Images were acquired using Abberior inverted microscope equipped with Olympus Plan-Apo 100×/1.40-NA oil objective and Avalanche Photodiode detector. Alexa Fluor 488 was excited by a 488-nm laser and star red was excited using a 640-nm laser. Two pulsed STED lasers were used (595 and 775 nm), and an Abberior Imspector was used for image acquisition.

Immunoisolation of syntaxin-6–positive membranes

Syntaxin-6–positive structures were isolated according to a protocol published elsewhere (Abu-Remaileh et al., 2017). Briefly, HEK-293 cells from three 15-cm plates were used for each condition. Cells were transfected with T7-SSTR2 alone or in combination with HA-EGFP-syntaxin-6. Cells were then treated with [D-Trp^8]-SOM for 60 min, rinsed twice with ice-cold PBS, scraped in 2 ml KPBS buffer (136 mM KCl and 10 mM KH_2PO_4, pH 7.25), and centrifuged at 2,000 rpm for 2 min in at 4°C. Pelleted cells were resuspended in 1 ml KPBS buffer. The cells were gently homogenized with 30 strokes of a 2-ml Dounce homogenizer. The homogenate was then centrifuged at 1,000 *g* for 3 min at 4°C to remove nuclei and cell debris. After discarding the pellet, the volume of the supernatant containing the cellular organelles was adjusted to 1 ml, and 25 µl was reserved as input. The remaining homogenate was incubated with 150 µl

KPBS prewashed anti-HA magnetic beads (Thermo Fisher Scientific) on a gentle rotator shaker for 3 min. After washing the beads three times with KPBS, the content of the immunoprecipitated syntaxin-6 structures was eluted by incubating the beads with 100 µl KPBS + 1% Triton X-100. The solubilized proteins were collected and separated by SDS-PAGE and probed by immunoblot.

Sucrose gradient fractionation

Gradient fractionation was performed as previously described (Waugh et al., 2003). Briefly, three 10-cm dishes of confluent AtT20 cells were placed on ice and washed twice with ice-cold PBS, pH 7.4. The cells were then washed with ice-cold 10 mM Tris/HCl, pH 7.4, to induce osmotic swelling. The osmotic buffer was quickly removed, and the cells were scraped into an ice-cold isotonic homogenization buffer composed of 10 mM Tris/HCl, 1 mM EGTA, 0.5 mM EDTA, 0.25 M sucrose, pH 7.4, and protease inhibitors (Roche). The cells were homogenized with several strokes of a loose-fitting Dounce homogenizer. The lysate was centrifuged for 5 min at 1,000 *g* and the postnuclear supernatants were collected. The postnuclear supernatant (2 ml) was fractionated on a 10-ml continuous 10–40% (wt/vol) sucrose density gradient centrifuged overnight at 180,000 *g*. Fractions (24 × 500 µl) were collected, beginning at the top of the gradient, and separated on SDS-PAGE, and different proteins were identified by immunoblot.

Generation of Rab10 knockout lines

For Rab10 knockout, LentiCRISPR v2 plasmid, which drives the expression of a single gRNA under the hU6 promoter, was used for cloning. The gRNA (5′-CACCGCGCCATTGGGAGGAGCGGCT-3′) targeting mouse Rab10 with BsmB1 overhangs were cloned into lentiCRISPR v2 as described previously (Shalem et al., 2014). Positive clones were confirmed by Sanger sequencing. For lentivirus production, Rab10-sgRNA lentivirus plasmid and packaging plasmids pMD2.G (plasmid #12259; Addgene) and psPAX2 (plasmid #12260; Addgene) were used at the ratio of 3:2:1. Culture supernatants were collected 72 h after transfection, filtered through a 0.45-µm syringe filter, centrifuged, and aliquoted at −80°C. Rab10 knockout cells were generated by transducing AtT20 cells with lentivirus and selected using blasticidin. Clonal selection was done by serial dilution, and clones positive for Rab10 knockout were screened by immunoblot.

Animals and experimental procedures

All animal procedures were approved by the Animal Care Committee of McGill University and conducted in compliance with the guidelines of the Canadian Council of Animal Care. Adult (8- to 10-wk-old) C57BL/6 mice (Charles River Canada) were group housed (n = 4) for 2 wk before the experiment under a 12-h light, 12-h dark cycle (lights on at 06:00 a.m.). During that time, the mice were habituated to the human handling 15 min each day to minimize stress at the day of experiment. Room temperature was maintained at 20 ± 2°C. Mice chow and tap water were available ad libitum. To determine the plasma GH levels, blood samples were collected for at least 2 h before sacrifice. Briefly, blood was collected from the tails of mice as 2-µl samples every 15–20 min starting at 9:00 a.m. as described previously (Steyn et al., 2011). All blood samples were immediately frozen at −80°C until GH levels were analyzed. For prediction of the time of apex and nadir of blood GH in mice, preliminary experiments were done to characterize the blood GH profile starting at 9:00 a.m. and ending at 15:00 p.m. Immediately after the last blood sample collection, the mice were anesthetized with an intraperitoneal injection of ketamine/xylazine/acepromazine followed by transaortic perfusion with 4% PFA in 0.1 M phosphate buffer, and pituitary glands were immediately extracted and immersed in the same fixative for 24 h at 4°C.

Tissue preparation

Once fixed, the pituitary glands were dehydrated in a graded ethanol series, embedded in paraffin, and serially sectioned at 4 µm thickness. Sections were subjected to antigen retrieval in Roche Benchmark ULTRA CC1 at 95°C for 64 min before sequential double immunolabeling for SSTR2 and GH or single labeling for either marker on consecutive sections. For double labeling of SSTR2 and GH, sections were incubated for 30 min at room temperature in a blocking solution containing 5% NGS and 2% BSA in PBS. Subsequently, sections were incubated overnight at 4°C with rabbit anti-SSTR2 antibody diluted 1:1,000 in a dilution buffer containing 0.2% NGS in PBS followed by three times washing with PBS and incubation with goat anti-rabbit IgG conjugated to Cy3 for 1 h at room temperature. That was followed by a second blocking step and incubation with a rabbit anti-GH antibody (catalog number ab126882; Abcam) conjugated to DyLight 488 using a DyLight 488 conjugation kit (catalog number ab201799; Abcam) according to the manufacturer's instructions. After final rinsing with PBS, the sections were mounted onto chrome-alum–coated slides using Aquapolymount (Polysciences). Slides were imaged using Zeiss LSM 710. The resulting images were cropped and adjusted for brightness and contrast using ImageJ.

GH assay

Plasma GH concentrations were measured in duplicate using a sensitive sandwich as described previously (Steyn et al., 2011). Briefly, a 96-well plate (Corning) was coated overnight at 4°C with 50 µl monkey anti-rat GH (rGH) antibody (AFP411S; National Institute of Diabetes and Digestive and Kidney Diseases-National Hormone and Pituitary Program [NIDDK-NHPP]) at a final dilution of 1:40,000). Each well was subsequently incubated with 200 µl blocking buffer (5% skim milk powder in PBS with Tween-20 [PBS-T; 0.05%]) for 2 h at room temperature. A standard curve was generated using a twofold serial dilution of mouse GH in PBS-T supplemented with BSA (0.2%, PBS-T/BSA). Standard curve or sample (50 µl) in duplicates were loaded and incubated for 2 h at room temperature with shaking. After washing, bound standards and samples were incubated with 50 µl of detection antibody (rabbit antiserum to rGH, AFP5672099, at a final dilution of 1:40,000; NIDDK-NHPP) for 90 min. The bound complex was incubated with 50 µl horseradish peroxidase–conjugated antibody (goat anti-rabbit, at a final dilution of 1:2,000; Bio-Rad) for 90 min. Addition of 100 µl O-phenylenediamine (00-2003; Invitrogen) substrate to each well resulted in an

enzymatic colorimetric reaction. This reaction was stopped by addition of 50 µl 3 M HCl, and the absorbance was read at a wavelength of 490 nm with a monochromatic microplate reader. The concentration of GH in each well was calculated by regression of the standard curve.

Image and statistical analysis

Pearson coefficient measurements were performed on a juxtanuclear ROI using Huygens Essential software (Scientific Volume Imaging) while Mander's coefficient measurements were done using the JACoP plugin in ImageJ (Bolte and Cordelières, 2006). In both cases, the juxtanuclear ROI was determined using the threshold function to pick the fluorescence signal of one channel and the colocalization function was used to determine if the signal of the other channel colocalize. Surface fluorescence intensity of SSTR2 in AtT20 cells was quantified in a ROI corresponding to the cell periphery using the hand drawing function in Zeiss ZEN lite software. The total fluorescence intensity was normalized for the cell circumference and the total bit depth. Quantification of at least 30–50 cells from three successive experiments was grouped. Data from at least three successive experiments were analyzed by one-factor ANOVA or two-factor ANOVA and Dunnett's, Tukey's, or Bonferroni comparison test procedures implemented in JMP statistical package (SAS Institute) or GraphPad Prism 5 as compared with nonstimulation condition. Data are presented as least-square means ± SEMs with treatment effects significant at $P < 0.05$.

Measurement of SSTR2 fluorescence in anterior pituitary cells from sections

Cell surface and cytoplasmic levels of SSTR2 were quantified essentially as per the method of Hanieh Toossi and colleagues (Toossi et al., 2018) using ZEN lite software. Briefly, a rectangular box of fixed size was placed over the plasma membrane and another box of the same size over the cytoplasm in each cell. The average fluorescence intensity was measured using the measure function in ZEN lite software. Cell surface to the intracellular ratios were calculated for each cell from 20 to 40 cells per hypophysis in 11 mice. Data were analyzed by Student's *t* test in GraphPad Prism 5. Data are presented as least-square means ± SEMs with treatment effects significant at $P < 0.05$.

Online supplemental material

Fig. S1 shows confocal images of AtT20 cells immunolabeled for SSTR2 and syntaxin-6 to highlight that the slow basal recycling dynamics of SSTR2 is not affected by Brefeldin A or cycloheximide treatments. Fig. S2 shows AtT20 cells immunolabeled for SSTR2 and syntaxin-6 or syntaxin-6 and PIST, PIST and TGN38 (positive control), or PIST and Giantin (negative control) following nocodazole treatment as a way to investigate false colocalization in confocal images. Fig. S3 A shows confocal images of parental AtT20 cells or Rab10 knockout lines, either control or expressing Rab10Q68L to show that the defect in SSTR2 recycling observed in the Rab10 knockout lines is restored when Rab10 was reintroduced, and Fig. S3 B shows confocal images of AtT20 cells expressing GLUT4 to highlight that Glut4 colocalizes to internalized SSTR2-positive structures. Fig. S4 shows confocal images of mouse pituitary somatotropes, at high or low blood GH levels, immunolabeled for SSTR2 or SSTR2 and GH. Fig. S5 shows confocal images of AtT20 cells transfected with siRNA against the indicated proteins to validate the antibodies. Video 1 shows confocal time lapse of HeLa cells transfected with EGFP-SSTR2 at basal levels. Video 2 shows confocal time lapse of HeLa cells transfected with EGFP-SSTR2 following [D-Trp^8]-SOM treatment. Video 3 shows confocal time lapse of HeLa cells transfected with EGFP-SSTR2 following [D-Trp^8]-SOM washout. Video 4 shows confocal time lapse of HeLa cells transfected with EGFP-SSTR2 and Ds-Red-syntaxin-6 following [D-Trp^8]-SOM washout. Video 5 shows a cropped area from Video 4 showing SSTR2 fusion at the plasma membrane. Video 6 shows confocal time lapse of HeLa cells transfected with EGFP-SSTR2 following [D-Trp^8]-SOM washout highlighting the recycling of SSTR2 on tubular carriers in HeLa cells. Video 7 shows confocal time lapse of HeLa cells transfected with EGFP-SSTR2 and mCherry-Rab8 following [D-Trp^8]-SOM washout. Video 8 shows confocal time lapse of HeLa cells transfected with EGFP-SSTR2 and mCherry-Rab13 following [D-Trp^8]-SOM washout. Video 9 shows confocal time-lapse of HeLa cells transfected with EGFP-SSTR2 and mCherry-Rab10 following [D-Trp^8]-SOM washout. Video 10 shows cropped area from Video 9 showing SSTR2/Rab10 cotrafficking and fusion of SSTR2 at the plasma membrane.

Acknowledgments

The authors thank Anne-Sophie Fratzscher and Sean Goldfarb for providing blind quantification. The authors wish to extend their gratitude to Linda Michel and Naomi Takeda for administrative assistance and Jacynthe Philie for technical assistance. The authors thank to the Histology Core Facility, McGill University, for pituitary procession and sectioning and for the Neuro Microscopy imaging facility.

This work was funded through a Canadian Institutes of Health Research foundation grant to P.S. McPherson, a Natural Sciences and Engineering Research Council grant to T. Stroh, and the Bachynski Family Foundation. W. Alshafie was supported by a Montreal Neurological Institute Jeanne Timmins Costello Fellowship and a Faculty of Medicine, McGill University Gerald Clavet and J.P. Giroud Fellowship. V. Francis was supported by a Fonds de recherche du Québec – Santé fellowship. P.S. McPherson is a James McGill Professor and a Fellow of the Royal Society of Canada.

The authors declare no competing financial interests.

Author contributions: W. Alshafie, P.S. McPherson, and T. Stroh designed all experiments, which were performed by W. Alshafie. W. Alshafie and P.S. McPherson generated the figures. V. Francis created Rab10 knockout cells and performed experiments pertaining to Fig. 8 B. K. Bednarz collected blood from mice and performed ELISAs to measure GH levels. Y.E. Pan assisted with experiments. W. Alshafie wrote the manuscript with T. Stroh and P.S. McPherson.

Submitted: 9 April 2019
Revised: 26 July 2019
Accepted: 25 October 2019

References

Abdullah, N., M. Beg, D. Soares, J.S. Dittman, and T.E. McGraw. 2016. Downregulation of a GPCR by β-Arrestin2-Mediated Switch from an Endosomal to a TGN Recycling Pathway. *Cell Reports.* 17:2966–2978. https://doi.org/10.1016/j.celrep.2016.11.050

Abu-Remaileh, M., G.A. Wyant, C. Kim, N.N. Laqtom, M. Abbasi, S.H. Chan, E. Freinkman, and D.M. Sabatini. 2017. Lysosomal metabolomics reveals V-ATPase- and mTOR-dependent regulation of amino acid efflux from lysosomes. *Science.* 358:807–813. https://doi.org/10.1126/science.aan6298

Allaire, P.D., A.L. Marat, C. Dall'Armi, G. Di Paolo, P.S. McPherson, and B. Ritter. 2010. The Connecdenn DENN domain: a GEF for Rab35 mediating cargo-specific exit from early endosomes. *Mol. Cell.* 37:370–382. https://doi.org/10.1016/j.molcel.2009.12.037

Aloisi, A.L., and C. Bucci. 2013. Rab GTPases-cargo direct interactions: fine modulators of intracellular trafficking. *Histol. Histopathol.* 28: 839–849.

Bao, S., R.M. Smith, L. Jarett, and W.T. Garvey. 1995. The effects of brefeldin A on the glucose transport system in rat adipocytes. Implications regarding the intracellular locus of insulin-sensitive Glut4. *J. Biol. Chem.* 270:30199–30204. https://doi.org/10.1074/jbc.270.50.30199

Belman, J.P., E.N. Habtemichael, and J.S. Bogan. 2014. A proteolytic pathway that controls glucose uptake in fat and muscle. *Rev. Endocr. Metab. Disord.* 15:55–66. https://doi.org/10.1007/s11154-013-9276-2

Bock, J.B., R.C. Lin, and R.H. Scheller. 1996. A new syntaxin family member implicated in targeting of intracellular transport vesicles. *J. Biol. Chem.* 271:17961–17965. https://doi.org/10.1074/jbc.271.30.17961

Bock, J.B., J. Klumperman, S. Davanger, and R.H. Scheller. 1997. Syntaxin 6 functions in trans-Golgi network vesicle trafficking. *Mol. Biol. Cell.* 8: 1261–1271. https://doi.org/10.1091/mbc.8.7.1261

Bolte, S., and F.P. Cordelières. 2006. A guided tour into subcellular colocalization analysis in light microscopy. *J. Microsc.* 224:213–232. https://doi.org/10.1111/j.1365-2818.2006.01706.x

Bowman, S.L., A.L. Soohoo, D.J. Shiwarski, S. Schulz, A.A. Pradhan, and M.A. Puthenveedu. 2015. Cell-autonomous regulation of Mu-opioid receptor recycling by substance P. *Cell Reports.* 10:1925–1936. https://doi.org/10.1016/j.celrep.2015.02.045

Brasselet, S., S. Guillen, J.P. Vincent, and J. Mazella. 2002. Beta-arrestin is involved in the desensitization but not in the internalization of the somatostatin receptor 2A expressed in CHO cells. *FEBS Lett.* 516:124–128. https://doi.org/10.1016/S0014-5793(02)02517-6

Chakrabarti, R., J. Buxton, M. Joly, and S. Corvera. 1994. Insulin-sensitive association of GLUT-4 with endocytic clathrin-coated vesicles revealed with the use of brefeldin A. *J. Biol. Chem.* 269:7926–7933.

Chege, N.W., and S.R. Pfeffer. 1990. Compartmentation of the Golgi complex: brefeldin-A distinguishes trans-Golgi cisternae from the trans-Golgi network. *J. Cell Biol.* 111:893–899. https://doi.org/10.1083/jcb.111.3.893

Cheung, N.W., and S.C. Boyages. 1995. Somatostatin-14 and its analog octreotide exert a cytostatic effect on GH3 rat pituitary tumor cell proliferation via a transient G0/G1 cell cycle block. *Endocrinology.* 136: 4174–4181. https://doi.org/10.1210/endo.136.10.7664634

Choquet, D. 2010. Fast AMPAR trafficking for a high-frequency synaptic transmission. *Eur. J. Neurosci.* 32:250–260. https://doi.org/10.1111/j.1460-9568.2010.07350.x

Cole, N.B., N. Sciaky, A. Marotta, J. Song, and J. Lippincott-Schwartz. 1996. Golgi dispersal during microtubule disruption: regeneration of Golgi stacks at peripheral endoplasmic reticulum exit sites. *Mol. Biol. Cell.* 7: 631–650. https://doi.org/10.1091/mbc.7.4.631

Csaba, Z., B. Lelouvier, C. Viollet, V. El Ghouzzi, K. Toyama, C. Videau, V. Bernard, and P. Dournaud. 2007. Activated somatostatin type 2 receptors traffic in vivo in central neurons from dendrites to the trans Golgi before recycling. *Traffic.* 8:820–834. https://doi.org/10.1111/j.1600-0854.2007.00580.x

Cuevas-Ramos, D., and M. Fleseriu. 2014. Somatostatin receptor ligands and resistance to treatment in pituitary adenomas. *J. Mol. Endocrinol.* 52: R223–R240. https://doi.org/10.1530/JME-14-0011

den Boon, F.S., and R.A. Sarabdjitsingh. 2017. Circadian and ultradian patterns of HPA-axis activity in rodents: Significance for brain functionality. *Best Pract. Res. Clin. Endocrinol. Metab.* 31:445–457. https://doi.org/10.1016/j.beem.2017.09.001

Durán-Pastén, M.L., and T. Fiordelisio. 2013. GnRH-Induced Ca(2+) Signaling Patterns and Gonadotropin Secretion in Pituitary Gonadotrophs. Functional Adaptations to Both Ordinary and Extraordinary Physiological Demands. *Front. Endocrinol. (Lausanne).* 4:127. https://doi.org/10.3389/fendo.2013.00127

Eigler, T., and A. Ben-Shlomo. 2014. Somatostatin system: molecular mechanisms regulating anterior pituitary hormones. *J. Mol. Endocrinol.* 53: R1–R19. https://doi.org/10.1530/JME-14-0034

Eikelboom, R., and G.S. Tannenbaum. 1983. Effects of obesity-inducing ventromedial hypothalamic lesions on pulsatile growth hormone and insulin secretion: evidence for the existence of a growth hormone-releasing factor. *Endocrinology.* 112:212–219. https://doi.org/10.1210/endo-112-1-212

Ferland, L., F. Labrie, M. Jobin, A. Arimura, and A.V. Schally. 1976. Physiological role of somatostatin in the control of growth hormone and thyrotropin secretion. *Biochem. Biophys. Res. Commun.* 68:149–156. https://doi.org/10.1016/0006-291X(76)90022-X

Fischer, T., C. Doll, S. Jacobs, A. Kolodziej, R. Stumm, and S. Schulz. 2008. Reassessment of sst2 somatostatin receptor expression in human normal and neoplastic tissues using the novel rabbit monoclonal antibody UMB-1. *J. Clin. Endocrinol. Metab.* 93:4519–4524. https://doi.org/10.1210/jc.2008-1063

Foley, K.P., and A. Klip. 2014. Dynamic GLUT4 sorting through a syntaxin-6 compartment in muscle cells is derailed by insulin resistance-causing ceramide. *Biol. Open.* 3:314–325. https://doi.org/10.1242/bio.20147898

Frohman, L.A., T.R. Downs, I.J. Clarke, and G.B. Thomas. 1990. Measurement of growth hormone-releasing hormone and somatostatin in hypothalamic-portal plasma of unanesthetized sheep. Spontaneous secretion and response to insulin-induced hypoglycemia. *J. Clin. Invest.* 86: 17–24. https://doi.org/10.1172/JCI114681

Glass, D.B., H.C. Cheng, L. Mende-Mueller, J. Reed, and D.A. Walsh. 1989. Primary structural determinants essential for potent inhibition of cAMP-dependent protein kinase by inhibitory peptides corresponding to the active portion of the heat-stable inhibitor protein. *J. Biol. Chem.* 264:8802–8810.

Hess, M.W., M. Müller, P.L. Debbage, M. Vetterlein, and M. Pavelka. 2000. Cryopreparation provides new insight into the effects of brefeldin A on the structure of the HepG2 Golgi apparatus. *J. Struct. Biol.* 130:63–72. https://doi.org/10.1006/jsbi.2000.4230

Ioannou, M.S., M. Girard, and P.S. McPherson. 2016. Rab13 Traffics on Vesicles Independent of Prenylation. *J. Biol. Chem.* 291:10726–10735. https://doi.org/10.1074/jbc.M116.722298

Jaldin-Fincati, J.R., M. Pavarotti, S. Frendo-Cumbo, P.J. Bilan, and A. Klip. 2017. Update on GLUT4 Vesicle Traffic: A Cornerstone of Insulin Action. *Trends Endocrinol. Metab.* 28:597–611. https://doi.org/10.1016/j.tem.2017.05.002

Jung, J.J., S.M. Inamdar, A. Tiwari, and A. Choudhury. 2012. Regulation of intracellular membrane trafficking and cell dynamics by syntaxin-6. *Biosci. Rep.* 32:383–391. https://doi.org/10.1042/BSR20120006

Lehmann, A., A. Kliewer, D. Schütz, F. Nagel, R. Stumm, and S. Schulz. 2014. Carboxyl-terminal multi-site phosphorylation regulates internalization and desensitization of the human sst2 somatostatin receptor. *Mol. Cell. Endocrinol.* 387:44–51. https://doi.org/10.1016/j.mce.2014.02.009

Lippincott-Schwartz, J., L. Yuan, C. Tipper, M. Amherdt, L. Orci, and R.D. Klausner. 1991. Brefeldin A's effects on endosomes, lysosomes, and the TGN suggest a general mechanism for regulating organelle structure and membrane traffic. *Cell.* 67:601–616. https://doi.org/10.1016/0092-8674(91)90534-6

Litvin, Y., M. Leiser, N. Fleischer, and J. Erlichman. 1986. Somatostatin inhibits corticotropin-releasing factor-stimulated adrenocorticotropin release, adenylate cyclase, and activation of adenosine 3′,5′-monophosphate-dependent protein kinase isoenzymes in AtT20 cells. *Endocrinology.* 119:737–745. https://doi.org/10.1210/endo-119-2-737

Lopez, F., J.P. Estève, L. Buscail, N. Delesque, N. Saint-Laurent, N. Vaysse, and C. Susini. 1996. Molecular mechanisms of antiproliferative effect of somatostatin: involvement of a tyrosine phosphatase. *Metabolism.* 45(8, Suppl 1):14–16. https://doi.org/10.1016/S0026-0495(96)90071-2

Luzio, J.P., B. Brake, G. Banting, K.E. Howell, P. Braghetta, and K.K. Stanley. 1990. Identification, sequencing and expression of an integral membrane protein of the trans-Golgi network (TGN38). *Biochem. J.* 270: 97–102. https://doi.org/10.1042/bj2700097

Martel, G., P. Dutar, J. Epelbaum, and C. Viollet. 2012. Somatostatinergic systems: an update on brain functions in normal and pathological aging. *Front Endocrinol (Lausanne).* 3:154. https://doi.org/10.3389/fendo.2012.00154

Martin, J.B., L.P. Renaud, and P. Brazeau Jr. 1974. Pulsatile growth hormone secretion: suppression by hypothalamic ventromedial lesions and by long-acting somatostatin. *Science.* 186:538–540. https://doi.org/10.1126/science.186.4163.538

Martin, S.K., R. Carroll, M. Benig, and D.F. Steiner. 1994. Regulation by glucose of the biosynthesis of PC2, PC3 and proinsulin in (ob/ob) mouse islets of Langerhans. *FEBS Lett.* 356:279–282. https://doi.org/10.1016/0014-5793(94)01284-9

Martin, S., G. Ramm, C.T. Lyttle, T. Meerloo, W. Stoorvogel, and D.E. James. 2000. Biogenesis of insulin-responsive GLUT4 vesicles is independent of brefeldin A-sensitive trafficking. *Traffic.* 1:652–660. https://doi.org/10.1034/j.1600-0854.2000.010809.x

Mundell, S.J., and J.L. Benovic. 2000. Selective regulation of endogenous G protein-coupled receptors by arrestins in HEK293 cells. *J. Biol. Chem.* 275:12900–12908. https://doi.org/10.1074/jbc.275.17.12900

Nouel, D., G. Gaudriault, M. Houle, T. Reisine, J.P. Vincent, J. Mazella, and A. Beaudet. 1997. Differential internalization of somatostatin in COS-7 cells transfected with SST1 and SST2 receptor subtypes: a confocal microscopic study using novel fluorescent somatostatin derivatives. *Endocrinology.* 138:296–306. https://doi.org/10.1210/endo.138.1.4834

Park, E.J., and T.H. Kwon. 2015. A Minireview on Vasopressin-regulated Aquaporin-2 in Kidney Collecting Duct Cells. *Electrolyte Blood Press.* 13:1–6. https://doi.org/10.5049/EBP.2015.13.1.1

Peverelli, E., E. Giardino, D. Treppiedi, M. Meregalli, M. Belicchi, V. Vaira, S. Corbetta, C. Verdelli, E. Verrua, A.L. Serban, et al. 2017. Dopamine receptor type 2 (DRD2) and somatostatin receptor type 2 (SSTR2) agonists are effective in inhibiting proliferation of progenitor/stem-like cells isolated from nonfunctioning pituitary tumors. *Int. J. Cancer.* 140:1870–1880. https://doi.org/10.1002/ijc.30613

Plotsky, P.M., and W. Vale. 1985. Patterns of growth hormone-releasing factor and somatostatin secretion into the hypophysial-portal circulation of the rat. *Science.* 230:461–463. https://doi.org/10.1126/science.2864742

Reaves, B., and G. Banting. 1992. Perturbation of the morphology of the trans-Golgi network following Brefeldin A treatment: redistribution of a TGN-specific integral membrane protein, TGN38. *J. Cell Biol.* 116:85–94. https://doi.org/10.1083/jcb.116.1.85

Reisine, T. 1990. Cellular mechanisms of somatostatin inhibition of calcium influx in the anterior pituitary cell line AtT-20. *J. Pharmacol. Exp. Ther.* 254:646–651.

Richardson, U.I., and A. Schonbrunn. 1981. Inhibition of adrenocorticotropin secretion by somatostatin in pituitary cells in culture. *Endocrinology.* 108:281–290. https://doi.org/10.1210/endo-108-1-281

Richardson, S.B., and S. Twente. 1993. Timing of exposure to somatostatin relative to growth hormone-releasing factor dictates the rat anterior pituitary cell growth hormone response. *J. Endocrinol.* 138:369–377. https://doi.org/10.1677/joe.0.1380369

Sano, H., L. Eguez, M.N. Teruel, M. Fukuda, T.D. Chuang, J.A. Chavez, G.E. Lienhard, and T.E. McGraw. 2007. Rab10, a target of the AS160 Rab GAP, is required for insulin-stimulated translocation of GLUT4 to the adipocyte plasma membrane. *Cell Metab.* 5:293–303. https://doi.org/10.1016/j.cmet.2007.03.001

Shalem, O., N.E. Sanjana, E. Hartenian, X. Shi, D.A. Scott, T. Mikkelson, D. Heckl, B.L. Ebert, D.E. Root, J.G. Doench, and F. Zhang. 2014. Genome-scale CRISPR-Cas9 knockout screening in human cells. *Science.* 343:84–87. https://doi.org/10.1126/science.1247005

Shewan, A.M., E.M. van Dam, S. Martin, T.B. Luen, W. Hong, N.J. Bryant, and D.E. James. 2003. GLUT4 recycles via a trans-Golgi network (TGN) subdomain enriched in Syntaxins 6 and 16 but not TGN38: involvement of an acidic targeting motif. *Mol. Biol. Cell.* 14:973–986. https://doi.org/10.1091/mbc.e02-06-0315

Sorkin, A., and M. von Zastrow. 2009. Endocytosis and signalling: intertwining molecular networks. *Nat. Rev. Mol. Cell Biol.* 10:609–622. https://doi.org/10.1038/nrm2748

Soya, H., and M. Suzuki. 1988. Somatostatin rapidly restores rat growth hormone (GH) release response attenuated by prior exposure to human GH-releasing factor in vitro. *Endocrinology.* 122:2492–2498. https://doi.org/10.1210/endo-122-6-2492

Soya, H., M. Suzuki, and M. Kato. 1990. Somatostatin pretreatment facilitates GRF-induced GH release and increase in free calcium in pituitary cells. *Biochem. Biophys. Res. Commun.* 172:276–281. https://doi.org/10.1016/S0006-291X(05)80205-0

Stachura, M.E., J.M. Tyler, and P.K. Farmer. 1988. Combined effects of human growth hormone (GH)-releasing factor-44 (GRF) and somatostatin (SRIF) on post-SRIF rebound release of GH and prolactin: a model for GRF-SRIF modulation of secretion. *Endocrinology.* 123:1476–1482. https://doi.org/10.1210/endo-123-3-1476

Steiner, R.A., J.K. Stewart, J. Barber, D. Koerker, C.J. Goodner, A. Brown, P. Illner, and C.C. Gale. 1978. Somatostatin: a physiological role in the regulation of growth hormone secretion in the adolescent male baboon. *Endocrinology.* 102:1587–1594. https://doi.org/10.1210/endo-102-5-1587

Steyn, F.J., and S.T. Ngo. 2017. Endocrine rhythms of growth hormone release: Insights from animal studies. *Best Pract. Res. Clin. Endocrinol. Metab.* 31:521–533. https://doi.org/10.1016/j.beem.2017.10.009

Steyn, F.J., L. Huang, S.T. Ngo, J.W. Leong, H.Y. Tan, T.Y. Xie, A.F. Parlow, J.D. Veldhuis, M.J. Waters, and C. Chen. 2011. Development of a method for the determination of pulsatile growth hormone secretion in mice. *Endocrinology.* 152:3165–3171. https://doi.org/10.1210/en.2011-0253

Stroh, T., A.C. Jackson, P. Sarret, C. Dal Farra, J.P. Vincent, H.J. Kreienkamp, J. Mazella, and A. Beaudet. 2000. Intracellular dynamics of sst5 receptors in transfected COS-7 cells: maintenance of cell surface receptors during ligand-induced endocytosis. *Endocrinology.* 141:354–365. https://doi.org/10.1210/endo.141.1.7259

Stroh, T., M.R. van Schouwenburg, A. Beaudet, and G.S. Tannenbaum. 2009. Subcellular dynamics of somatostatin receptor subtype 1 in the rat arcuate nucleus: receptor localization and synaptic connectivity vary in parallel with the ultradian rhythm of growth hormone secretion. *J. Neurosci.* 29:8198–8205. https://doi.org/10.1523/JNEUROSCI.0336-09.2009

Strowski, M.Z., M.P. Dashkevicz, R.M. Parmar, H. Wilkinson, M. Kohler, J.M. Schaeffer, and A.D. Blake. 2002. Somatostatin receptor subtypes 2 and 5 inhibit corticotropin-releasing hormone-stimulated adrenocorticotropin secretion from AtT-20 cells. *Neuroendocrinology.* 75:339–346. https://doi.org/twbch=":"

Sun, Y., P.J. Bilan, Z. Liu, and A. Klip. 2010. Rab8A and Rab13 are activated by insulin and regulate GLUT4 translocation in muscle cells. *Proc. Natl. Acad. Sci. USA.* 107:19909–19914. https://doi.org/10.1073/pnas.1009523107

Sun, Y., J. Jaldin-Fincati, Z. Liu, P.J. Bilan, and A. Klip. 2016. A complex of Rab13 with MICAL-L2 and α-actinin-4 is essential for insulin-dependent GLUT4 exocytosis. *Mol. Biol. Cell.* 27:75–89. https://doi.org/10.1091/mbc.E15-05-0319

Tallent, M., G. Liapakis, A.M. O'Carroll, S.J. Lolait, M. Dichter, and T. Reisine. 1996. Somatostatin receptor subtypes SSTR2 and SSTR5 couple negatively to an L-type Ca2+ current in the pituitary cell line AtT-20. *Neuroscience.* 71:1073–1081. https://doi.org/10.1016/0306-4522(95)00510-2

Tannenbaum, G.S. 1993. Genesis of episodic growth hormone secretion. *J. Pediatr. Endocrinol. Metab.* 6:273–282. https://doi.org/10.1515/JPEM.1993.6.3-4.273

Tannenbaum, G.S., and N. Ling. 1984. The interrelationship of growth hormone (GH)-releasing factor and somatostatin in generation of the ultradian rhythm of GH secretion. *Endocrinology.* 115:1952–1957. https://doi.org/10.1210/endo-115-5-1952

Tannenbaum, G.S., R. Eikelboom, and N. Ling. 1983. Human pancreas GH-releasing factor analog restores high-amplitude GH pulses in CNS lesion-induced GH deficiency. *Endocrinology.* 113:1173–1175. https://doi.org/10.1210/endo-113-3-1173

Tannenbaum, G.S., J.C. Painson, M. Lapointe, W. Gurd, and G.F. McCarthy. 1990. Interplay of somatostatin and growth hormone-releasing hormone in genesis of episodic growth hormone secretion. *Metabolism.* 39(9, Suppl 2):35–39. https://doi.org/10.1016/0026-0495(90)90206-R

Tannenbaum, G.S., F. Farhadi-Jou, and A. Beaudet. 1993. Ultradian oscillation in somatostatin binding in the arcuate nucleus of adult male rats. *Endocrinology.* 133:1029–1034. https://doi.org/10.1210/endo.133.3.8103446

Terry, L.C., and J.B. Martin. 1981. The effects of lateral hypothalamic-medial forebrain stimulation and somatostatin antiserum on pulsatile growth hormone secretion in freely behaving rats: evidence for a dual regulatory mechanism. *Endocrinology.* 109:622–627. https://doi.org/10.1210/endo-109-2-622

Tie, H.C., D. Mahajan, B. Chen, L. Cheng, A.M. VanDongen, and L. Lu. 2016. A novel imaging method for quantitative Golgi localization reveals differential intra-Golgi trafficking of secretory cargoes. *Mol. Biol. Cell.* 27:848–861. https://doi.org/10.1091/mbc.E15-09-0664

Tojo, K., and A.B. Abou-Samra. 1993. Corticotropin-releasing factor (CRF) stimulates 45Ca2+ uptake in the mouse corticotroph cell line AtT-20. *Life Sci.* 52:621–630. https://doi.org/10.1016/0024-3205(93)90453-A

Toossi, H., E. Del Cid-Pellitero, and B.E. Jones. 2018. Homeostatic Changes in GABA and Acetylcholine Muscarinic Receptors on GABAergic Neurons in the Mesencephalic Reticular Formation following Sleep Deprivation. *eNeuro.* 4: ENEURO.0269-17.2017.

Tooze, J., and M. Hollinshead. 1992. In AtT20 and HeLa cells brefeldin A induces the fusion of tubular endosomes and changes their distribution and some of their endocytic properties. *J. Cell Biol.* 118:813–830. https://doi.org/10.1083/jcb.118.4.813

Trischler, M., W. Stoorvogel, and O. Ullrich. 1999. Biochemical analysis of distinct Rab5- and Rab11-positive endosomes along the transferrin pathway. *J. Cell Sci.* 112:4773–4783.

Tulipano, G., R. Stumm, M. Pfeiffer, H.J. Kreienkamp, V. Höllt, and S. Schulz. 2004. Differential beta-arrestin trafficking and endosomal sorting of somatostatin receptor subtypes. *J. Biol. Chem.* 279:21374–21382. https://doi.org/10.1074/jbc.M313522200

Varner, M.A., S.L. Davis, and J.J. Reeves. 1980. Temporal serum concentrations of growth hormone, thyrotropin, insulin, and glucagon in sheep immunized against somatostatin. *Endocrinology*. 106:1027–1032. https://doi.org/10.1210/endo-106-3-1027

Vazirani, R.P., A. Verma, L.A. Sadacca, M.S. Buckman, B. Picatoste, M. Beg, C. Torsitano, J.H. Bruno, R.T. Patel, K. Simonyte, et al. 2016. Disruption of Adipose Rab10-Dependent Insulin Signaling Causes Hepatic Insulin Resistance. *Diabetes.* 65:1577–1589. https://doi.org/10.2337/db15-1128

Vistein, R., and M.A. Puthenveedu. 2013. Reprogramming of G protein-coupled receptor recycling and signaling by a kinase switch. *Proc. Natl. Acad. Sci. USA.* 110:15289–15294. https://doi.org/10.1073/pnas.1306340110

Wagner, M., A.K. Rajasekaran, D.K. Hanzel, S. Mayor, and E. Rodriguez-Boulan. 1994. Brefeldin A causes structural and functional alterations of the trans-Golgi network of MDCK cells. *J. Cell Sci.* 107:933–943.

Waugh, M.G., S. Minogue, J.S. Anderson, A. Balinger, D. Blumenkrantz, D.P. Calnan, R. Cramer, and J.J. Hsuan. 2003. Localization of a highly active pool of type II phosphatidylinositol 4-kinase in a p97/valosin-containing-protein-rich fraction of the endoplasmic reticulum. *Biochem. J.* 373: 57–63. https://doi.org/10.1042/bj20030089

Wehrenberg, W.B., P. Brazeau, R. Luben, P. Böhlen, and R. Guillemin. 1982. Inhibition of the pulsatile secretion of growth hormone by monoclonal antibodies to the hypothalamic growth hormone releasing factor (GRF). *Endocrinology*. 111:2147–2148. https://doi.org/10.1210/endo-111-6-2147

Wendler, F., and S. Tooze. 2001. Syntaxin 6: the promiscuous behaviour of a SNARE protein. *Traffic.* 2:606–611. https://doi.org/10.1034/j.1600-0854.2001.20903.x

Wood, S.A., J.E. Park, and W.J. Brown. 1991. Brefeldin A causes a microtubule-mediated fusion of the trans-Golgi network and early endosomes. *Cell.* 67:591–600. https://doi.org/10.1016/0092-8674(91)90533-5

Yao, R., T. Maeda, S. Takada, and T. Noda. 2001. Identification of a PDZ domain containing Golgi protein, GOPC, as an interaction partner of frizzled. *Biochem. Biophys. Res. Commun.* 286:771–778. https://doi.org/10.1006/bbrc.2001.5430

Zhao, P., M. Canals, J.E. Murphy, D. Klingler, E.M. Eriksson, J.C. Pelayo, M. Hardt, N.W. Bunnett, and D.P. Poole. 2013. Agonist-biased trafficking of somatostatin receptor 2A in enteric neurons. *J. Biol. Chem.* 288: 25689–25700. https://doi.org/10.1074/jbc.M113.496414

Zhou, X., P. Shentu, and Y. Xu. 2017. Spatiotemporal Regulators for Insulin-Stimulated GLUT4 Vesicle Exocytosis. *J. Diabetes Res.* 2017:1683678. https://doi.org/10.1155/2017/1683678

Supplemental material

Alshafie et al., https://doi.org/10.1083/jcb.201904054

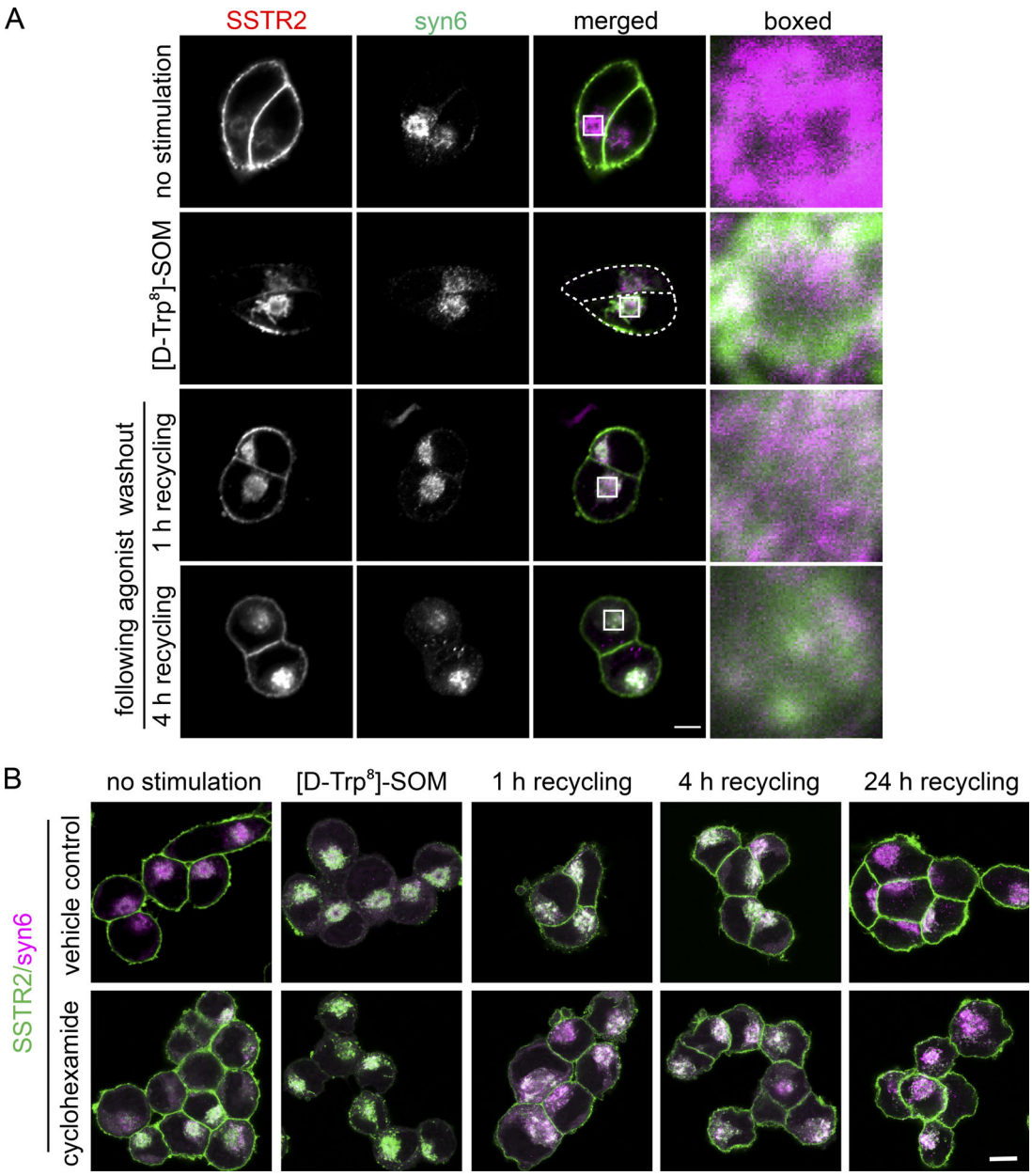

Figure S1. **SSTR2 displays slow recycling dynamics in the presence of Brefeldin A and cycloheximide. (A)** AtT20 cells were incubated for 40 min without (no stimulation) or with 100 nM [D-Trp^8]-SOM in the presence of 10 µM Brefeldin A and then fixed and processed for immunofluorescence with antibodies recognizing SSTR2 or syntaxin-6 (top two rows of panels). In parallel, cells treated with 100 nM [D-Trp^8]-SOM for 40 min in the presence of Brefeldin A were subsequently transferred to 4°C, surface-bound agonist was stripped by brief acid wash, and the cells were returned to 37°C for 1 or 4 h before being processed for immunofluorescence with antibodies recognizing SSTR2 or syntaxin-6 (bottom two rows of panels). The boxes in the merged images are shown at higher magnification on the far right. Scale bars represent 5 µm and 1 µm for the low- and high-magnification images, respectively. Dashed line indicates cell boundaries. **(B)** AtT20 cells were incubated with DMSO or 100 µg/ml cycloheximide 2 h before the start of experiment. Th cells were then incubated for 40 min without (no stimulation) or with 100 nM [D-Trp^8]-SOM in the presence of vehicle control or cycloheximide (left 4 most panels). In parallel, cells treated with [D-Trp^8]-SOM were subsequently transferred to 4°C, surface-bound agonist was stripped by a brief acid wash, and the cells were returned to 37°C for 1, 4, and 24 h (right six most panels). In all cases, at the end of the incubations cells were processed for immunofluorescence with antibodies recognizing SSTR2 or syntaxin-6. Scale bar represents 5 µm.

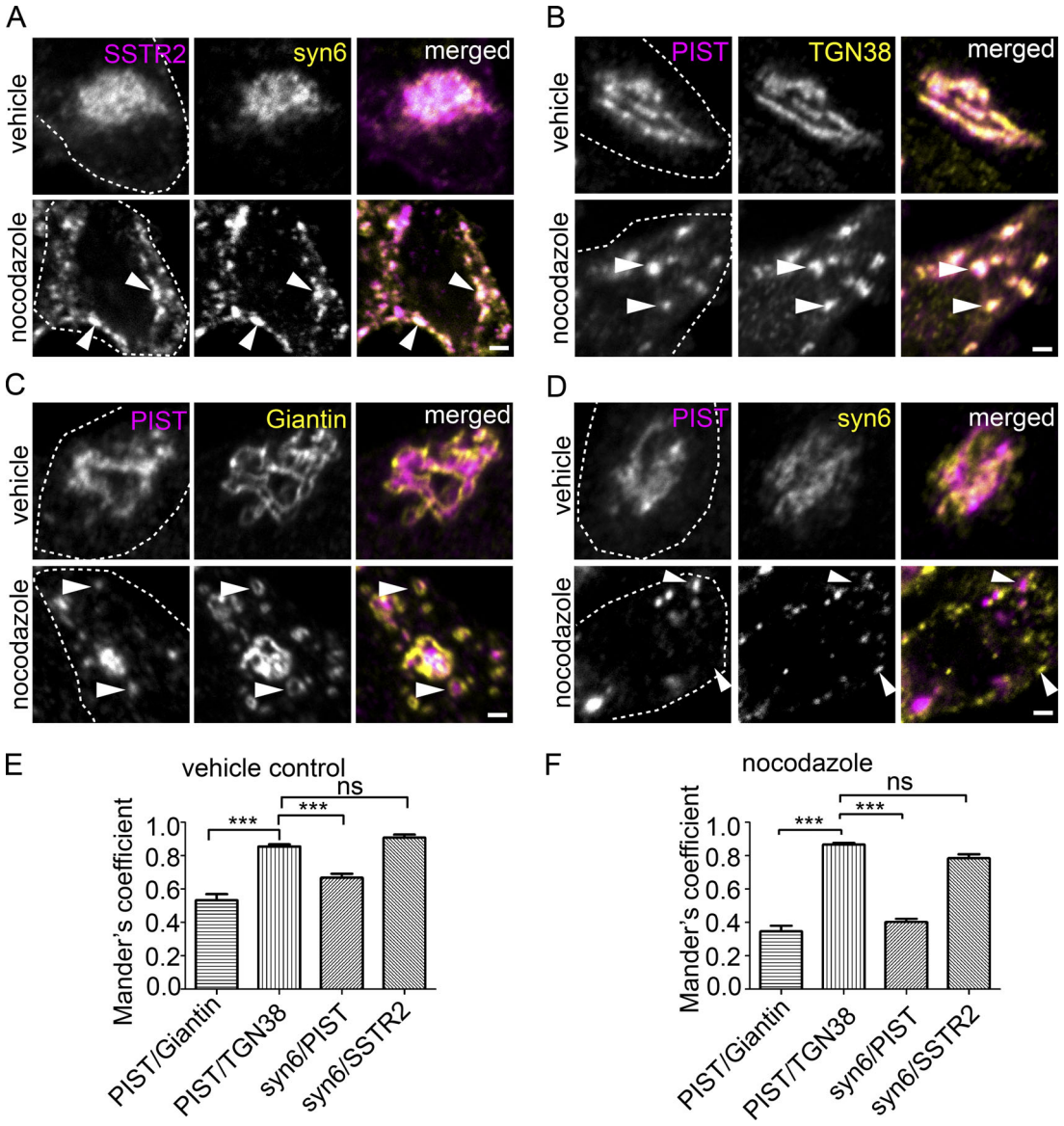

Figure S2. **SSTR2 and syntaxin-6 remain colocalized under nocodazole treatment. (A)** AtT20 cells were treated with vehicle or 20 µM nocodazole for 2 h in DMEM and for the last 40 min of the nocodazole treatment with 100 nM [D-Trp^8]-SOM before being fixed and processed for immunofluorescence with antibodies against the indicated proteins. **(B–D)** AtT20 cells were treated with vehicle or 20 µM nocodazole for 2 h in DMEM before being fixed and processed for immunofluorescence with antibodies against the indicated proteins. The arrowheads in A and B point to colocalizing structures, while the arrowheads in C and D point to noncolocalizing structures. Scale bars represent 1 µm. Dashed lines indicate cell boundaries. **(E and F)** Mander's correlation coefficient measurements of at least 30–40 cells from two or three independent experiments for cells treated with vehicle (E) or nocodazole (F). Data were analyzed by one-factor ANOVA and Tukey comparison test (procedures implemented in the GraphPad Prism 5 statistical package). Data are presented as least-square means ± SEMs with treatment effects significant at ***, $P < 0.001$.

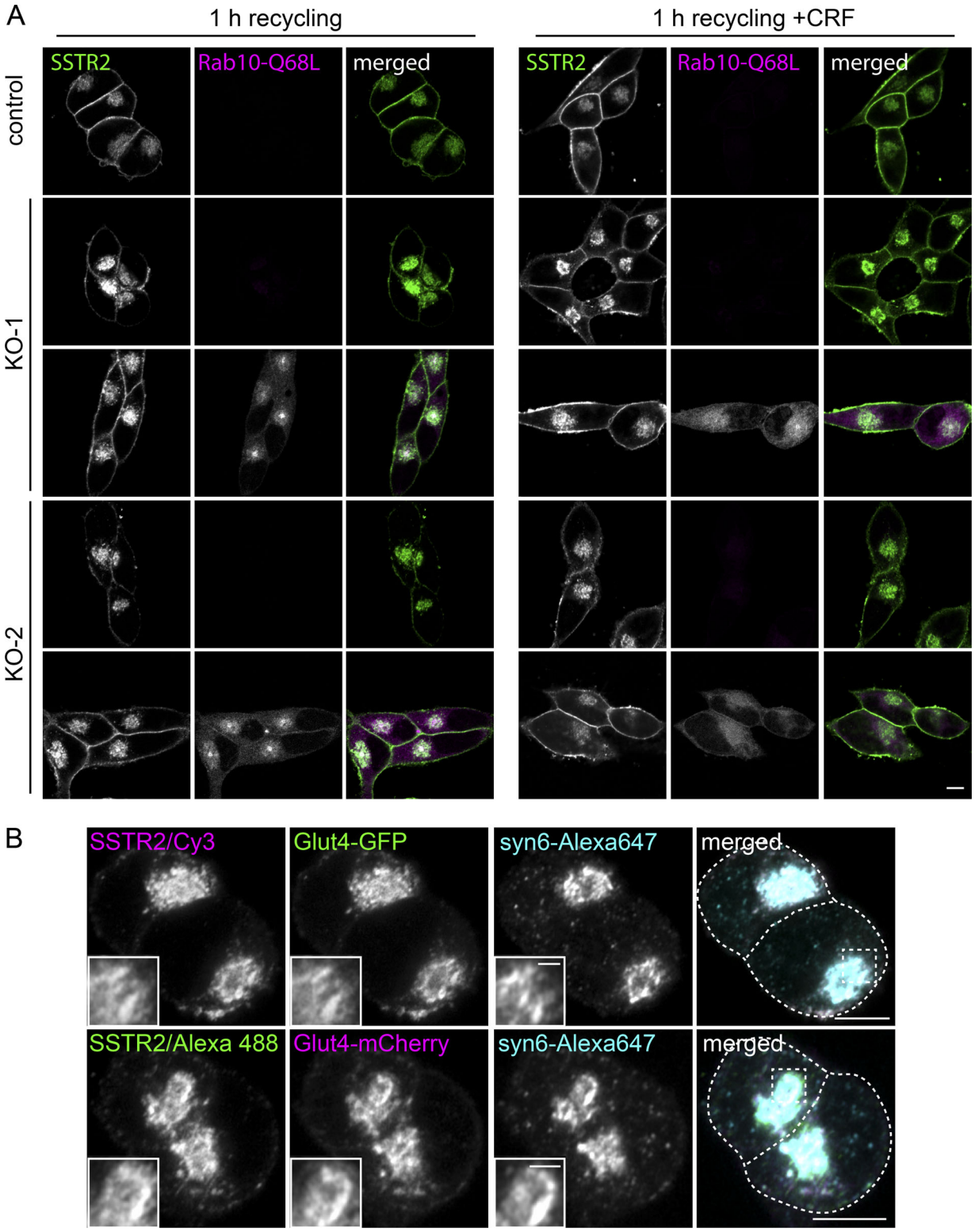

Figure S3. **SSTR2 is in a vesicle that requires Rab10 for recycling and is positive for transfected GLUT4. (A)** Control AtT20 cells or the two Rab10 knockout lines (KO-1 and KO-2) were electroporated with 5 µg EGFP-Rab10Q68L. At 72 h after transfection, cells were treated for 60 min with [D-Trp^8]-SOM to induce maximal SSTR2 internalization followed by brief acid wash and incubation in ligand-free media for 1 h at 37°C without or with 100 nM CRF. After the treatments, cells were fixed and processed for immunofluorescence with antibody recognizing SSTR2. Scale bar represents 5 µm. **(B)** GLUT4 is sorted to GLSVs in AtT20 cells. AtT20 cells were electroporated with 5 µg GLUT4-GFP or GLUT4-mCherry. 24 h after transfection, cells were treated for 40 min with [D-Trp^8]-SOM and then fixed and processed for immunofluorescence with antibody recognizing SSTR2 and syntaxin-6. Scale bars represent 5 µm and 1 µm for the low- and high-magnification images, respectively.

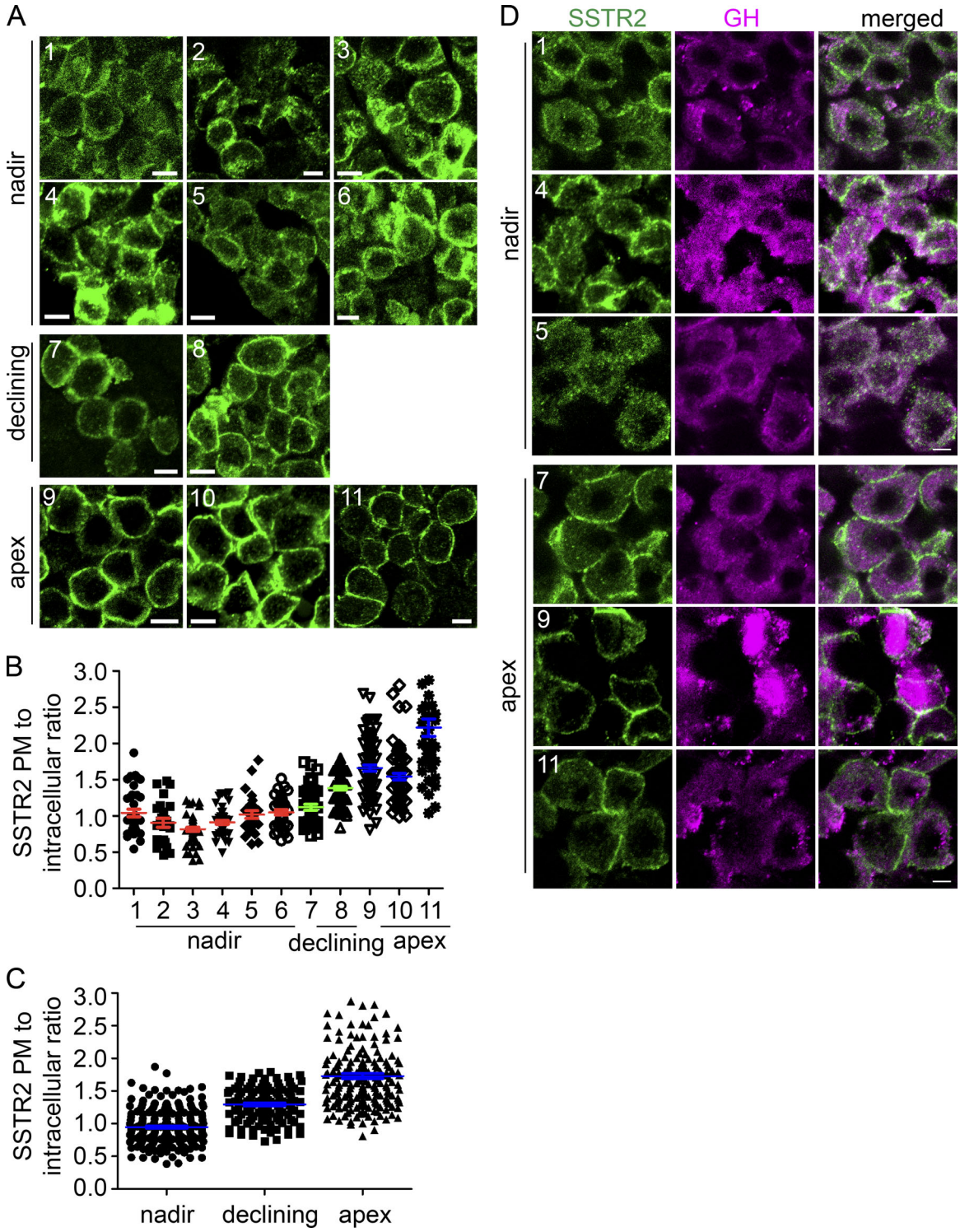

Figure S4. **Analysis of the SSTR2 surface to intracellular ratio in mouse pituitary. (A)** SSTR2 staining in sections of pituitary with blood GH levels at the nadir, declining or at the apex as indicated. The mouse number is stated on each panel and corresponds to the GH profiles shown in Fig. 10 C. Scale bars represent 5 µm. **(B and C)** The cell surface to intracellular ratio of SSTR2 immunofluorescent signal from individual cells from individual animals (B) or grouped depending on the GH status (C). PM, plasma membrane. **(D)** Sections of pituitary glands from selected mice as indicated were immunostained with antibodies recognizing SSTR2 and GH. The mice were selected from the animals that were sacrificed at the apex or nadir of blood GH levels. Scale bars represent 5 µm.

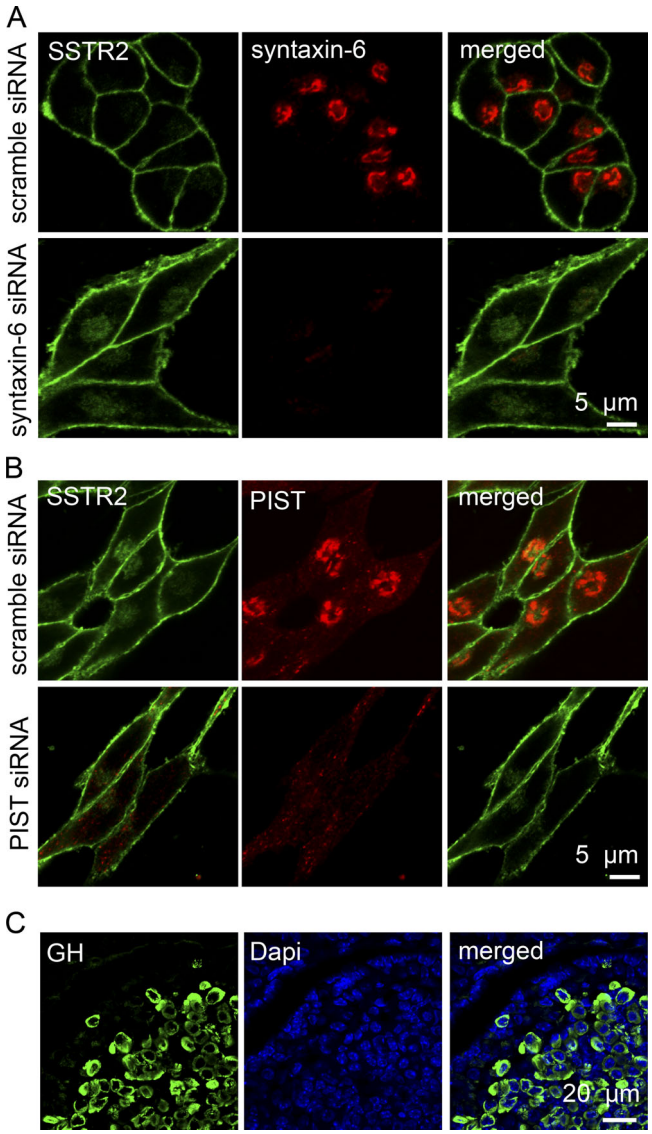

Figure S5. **Antibody validation.** Validation of syntaxin-6 (A) and PIST (B) antibodies was done using predesigned siRNA directed against mouse syntaxin-6 (FlexiTube siRNA, NM-021433, #SI02674231, and #S102717729; Qiagen) or PIST (FlexiTube siRNA, NM-001199272, #SI01054900; Qiagen). AtT20 cells were transfected with 50 nM of siRNA 48 h before immunostaining for the indicating proteins. Note the disappearance of the immunofluorescent signal in the siRNA-transfected cells, but not in the cells transfected with a scrambled siRNA. **(C)** GH antibody was tested on a pituitary section showing selective staining of a subset of pituitary cells.

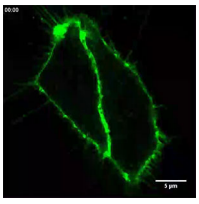

Video 1. **HeLa cells transfected with EGFP-SSTR2 were imaged for 5 min at the basal levels.** Frames were obtained using a Zeiss LSM 880 microscope with an airyscan at 10-s intervals.

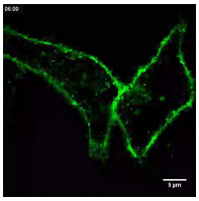

Video 2. **HeLa cells transfected with EGFP-SSTR2 were imaged 6 min after applying 100 nM of [D-Trp^8]-SOM for 42 min at 10-s intervals using a Zeiss LSM 880 microscope with an airyscan.**

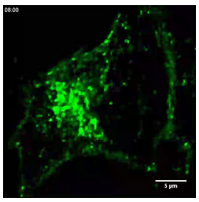

Video 3. **HeLa cells transfected with EGFP-SSTR2 were stimulated for 60 min with 100 nM of [D-Trp^8]-SOM.** Cells were imaged 8 min following ligand washout for 22 min at 10-s intervals using a Zeiss LSM 880 microscope with an airyscan.

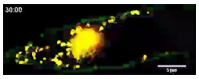

Video 4. **HeLa cells were transfected with EGFP-SSTR2 (green) and Ds-Red-syntaxin-6 (red).** Cells were stimulated for 60 min with 100 nM of [D-Trp^8]-SOM. Cells were imaged 30 min following ligand washout for 27 min using a Zeiss LSM 880 microscope with airyscan at 20-s intervals.

Video 5. **Cropped area from Video 4 showing SSTR2 fusion at the plasma membrane.** Upon reaching the plasma membrane, the syntaxin-6–positive vesicles of SSTR2 can be seen to come in contact with the surface followed by the insertion of SSTR2 into the plasma membrane, while syntaxin-6 remains on the cytoplasmic side of the plasma membrane. Cells were imaged as in Video 4.

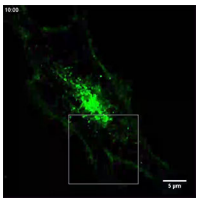

Video 6. **HeLa cells transfected with EGFP-SSTR2 were stimulated for 60 min with 100 nM of [D-Trp^8]-SOM.** Cells were imaged 10 min following ligand washout for 15 min at 20-s intervals using a Zeiss LSM 880 microscope with an airyscan. Note the recycling of SSTR2 on tubular carriers.

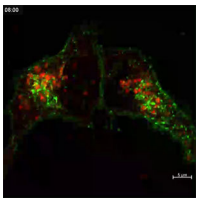

Video 7. **HeLa cells transfected with EGFP-SSTR2 and mCherry-Rab8 were stimulated for 60 min with 100 nM of [D-Trp^8]-SOM.** Cells were imaged 8 min following ligand washout for 28 min at 20-s intervals using a Zeiss LSM 880 microscope with an airyscan. Note the absence of colocalization of SSTR2 with Rab8.

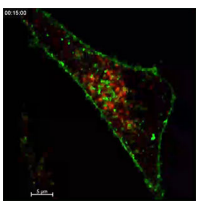

Video 8. **HeLa cells transfected with EGFP-SSTR2 and mCherry-Rab13 were stimulated for 60 min with 100 nM of [D-Trp^8]-SOM.** Cells were imaged 12 min following ligand removal for 15 min at 10-s intervals using a Zeiss LSM 880 microscope with airyscan. Note the absence of colocalization of SSTR2 with Rab13.

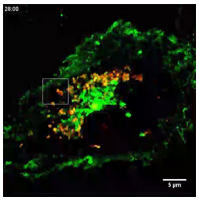

Video 9. **HeLa cells transfected with EGFP-SSTR2 and mCherry-Rab10 were stimulated for 60 min with 100 nM of [D-Trp^8]-SOM.** Cells were imaged 28 min following ligand removal at 20-s intervals using a Zeiss LSM 880 microscope with airyscan. Note colocalization of SSTR2 with Rab10.

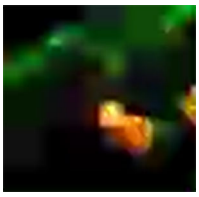

Video 10. **Cropped area from Video 9 showing SSTR2/Rab10 cotrafficking and fusion of SSTR2 at the plasma membrane.** Cells were imaged as in Video 9.